Monte Carlo studies of the ordering of ceramic superconductors: Chiral-glass, orbital-glass, and nonlinear susceptibilities

Hikaru Kawamura and Mai Suan Li*
Faculty of Engineering and Design, Kyoto Institute of Technology, Sakyo-ku, Kyoto 606, Japan
(Received 26 October 1995; revised manuscript received 15 March 1996)

Static and dynamic properties of the intergranular ordering of ceramic superconductors are studied by Monte Carlo simulations on a three-dimensional lattice model of a Josephson-junction array with finite self-inductance. Both cases of d-wave and s-wave pairing symmetries are studied. In the case of d-wave ceramics, intrinsic frustration effects combined with quenched randomness lead to the glassy behavior reminiscent of the spin glass even in zero magnetic field. It is found that the zero-field nonlinear susceptibility exhibits a negatively divergent behavior, suggesting the occurrence of a cooperative transition into an ordered state characterized by the random freezing of chirality or flux. In this ''chiral-glass'' state, global Z_2 time-reversal symmetry appears to be broken spontaneously with keeping the $U(1)$ gauge symmetry. Dynamic simulations on the linear ac susceptibility suggest that d-wave ceramics exhibits much stronger dissipation than s-wave ceramics in the low-frequency regime. In the case of s-wave ceramics, standard superconducting transitions with broken $U(1)$ gauge symmetry occurs where nonlinear susceptibility exhibits only a very weak anomaly. Implications to experiments on high-T_c ceramics are discussed. [S0163-1829(96)07725-9]

I. INTRODUCTION

There has been a continual interest in the ordering phenomena of ceramic or granular superconductors both from experimental and theoretical sides. Ceramic superconductors are often modeled as a weakly coupled random Josephson network consisting of superconducting grains. Recently, interest in these materials has been renewed by the discovery of high-T_c superconductors, since these cuprate materials are often ceramics. In fact, soon after the experimental discovery of high-T_c superconductors Ba-La-Cu-O, Müller, Takashige, and Bednorz reported that this material exhibits a glassy behavior reminiscent of the spin glass.[1] Although many experimentalists have continuously observed a close analogy to the spin glass since then,[2–4] true origin of the observed spin-glass-like behavior in ceramic high-T_c superconductors has yet to be clarified.

In recent years, there accumulated a considerable amount of experimental evidence that high-T_c cuprate superconductors are ''anisotropic'' or unconventional superconductors with the non-s-wave pairing symmetry.[5–7] Most promising pairing symmetry appears to be $d_{x^2-y^2}$, with four nodes on the Fermi surface. Naturally, such anisotropic nature of the superconducting order parameter is expected to have a profound effect on the ordering of ceramic systems because the property of Josephson junctions is sensitive to the phase difference of the Cooper-pair wave functions on both sides of the junction. In particular, if the crystallographic a and b axes are connected at the junction, the Cooper pair acquires a phase shift of π across the junction (π junction).[8] One may also regard the π junction as a junction with a *negative* Josephson coupling $J<0$. This should be contrasted to the standard 0 junction with a positive Josephson coupling $J>0$.

Sigrist and Rice invoked such π junctions arising from the $d_{x^2-y^2}$ pairing symmetry as a physical origin of the paramagnetic behavior observed experimentally in some high-T_c compounds (paramagnetic Meissner effect). When one measures the field-cooled susceptibility $\chi_{\rm FC}$ in small dc fields for certain high-T_c samples, $\chi_{\rm FC}$ becomes *positive* at low temperatures, quite contrary to the standard Meissner effect.[9–11] Meanwhile, the zero-field-cooled susceptibility $\chi_{\rm ZFC}$ remains always negative. The frustration effect inherent to odd rings consisting of such π junctions gives rise to spontaneous circulating supercurrent and orbital moment even in zero external field, which may cause the paramagnetic behavior observed experimentally.

In fact, the appearance of spontaneous supercurrents and the paramagnetic behavior had been anticipated by several theorists prior to the experimental observation of the paramagnetic Meissner effect (PME), although in these earlier theoretical studies this was not necessarily related to the unconventional pairing symmetry.[12–15] Kusmartsev called a state in ceramic superconductors characterized by orbital paramagnetism and superconductivity an ''orbital-glass'' state.[15] A recent numerical simulation on an orbital-glass model by Domínguez, Jagla, and Balseiro has successfully reproduced the paramagnetic behavior observed experimentally.[16]

However, the true nature of an ''orbital-glass state'' and of an ''orbital-glass transition'' still remains largely ambiguous. The picture by Sigrist and Rice is essentially a single-loop picture in which the interactions between loops are irrelevant.[8] In their scenario, when the temperature is lowered across the superconducting transition temperature of each grain $T_c^{\rm gr}$, $\chi_{\rm FC}$ changes its sign from negative to positive at a certain temperature, T_0, slightly below $T_c^{\rm gr}$. It should be noted that such a change of sign of $\chi_{\rm FC}$, which is often regarded as a measure of the orbital-glass transition point, is a crossover not related to any intergranular (interloop) cooperative phenomena. In this picture, the PME arises as a property of an ensemble of noninteracting loops if there occurs an *intragranular* superconducting transition. In fact,

many of the experimental results on the PME for Bi-Sr-Ca-Cu-O appear to be explained on the basis of such independent loop picture.[17] By contrast, the possible cooperative character of the orbital-glass state was pointed out by Domínguez, Jagla, and Balseiro[16] and by Khomskii,[10] although these authors did not detail the nature of the cooperative phenomena.

Naturally, one may ask here whether there could be a thermodynamically stable orbital-glass state characterized by a spontaneous breaking of certain symmetry over an entire granular system. An issue to be addressed is whether there could be some sort of thermodynamic *intergranular* phase transition accompanied with a divergent length scale over grains, and if it is, what is the order parameter of such phase transition.

Recently, on the basis of an analogy to the three-dimensional XY spin glass,[18] one of the present authors (H.K.) claimed that so long as the screening effects could be neglected, a sharp thermodynamic phase transition might indeed occur.[23] In this scenario, a possible ordered state of d-wave ceramic superconductors was associated with a recently proposed *chiral-glass* state of an XY spin glass:[24–26] In the chiral-glass state of an XY spin glass, only spin *chiralities* are frozen randomly, while XY spins remain disordered (chirality is an Ising-like quantity representing the sense or the handedness of the noncollinear spin structures[27]), leading to a spontaneous breaking of spin-reflection symmetry $[Z_2]$ with keeping spin-rotation symmetry $[SO(2)]$. In terms of d-wave ceramics, such a chiral-glass state is an ordered phase *with a spontaneously broken* Z_2 *time-reversal symmetry*, but it is not a true superconductor in the strict sense since the $U(1)=SO(2)$ gauge symmetry is *not* broken even randomly on sufficiently long length and time scales. It was also shown[23] that an external magnetic field in an Josephson-junction array works as a field conjugate to the chirality (chiral field), and as a consequence, the zero-field *nonlinear* susceptibility χ_2 exhibits a negative divergence at the transition point. Since the nature of the ordered state proposed in Ref. 23 is different from the orbital-glass state in a single-loop picture,[8,15,17] something like *spin glasses* versus *superparamagnets*, we will call the former the chiral-glass state when the distinction between the two pictures should be better clarified.

It should be emphasized that in Ref. 23 the screening effects were totally neglected. It is not clear at the present stage how the thermodynamic properties are affected by the screening effects. In the present paper, we address this question simulating the three-dimensional lattice model of ceramic superconductors with finite self-inductance. The model studied is the same as the one studied by previous authors, in particular the model studied by Domínguez, Jagla, and Balseiro.[16] However, we extend their calculations in several ways. First, nonlinear susceptibilities are calculated in addition to linear susceptibilities which are expected to be the most sensitive probe of the possible chiral-glass order. Several other quantities related to chiral order, including chirality and flux, are also calculated. Second, we make simulations both for d-wave and s-wave ceramics in parallel, and make comparison between the two results, aimed at clarifying how the difference in the pairing symmetry would show up in the thermodynamic properties of ceramic superconductors. Third, we study not only static properties but also dynamic properties like linear ac susceptibilities, including its imaginary part.

In the present Monte Carlo simulation, we will not pay much attention to the equilibration problem, and the data are only those obtained within a finite observation-time window. Thus, main interest in the present paper is not to determine whether there exists an equilibrium chiral-glass transition, which will be left to the future work, but rather to see in light of the possible chiral-glass ordering how various thermodynamic properties behave in the presence of screening.

The remainder of this paper is organized as follows. In Sec. II, we introduce our model and physical quantities of interest. Symmetry properties of the Hamiltonian in zero and nonzero magnetic fields are analyzed, and the important meaning of chirality is clarified. Technical details of our simulations are also given here. In Sec. III, results of simulations on static properties in zero external field are presented both for s-wave and d-wave models. Linear and nonlinear dc susceptibilities, chirality and flux are calculated for several typical values of the inductance. Results of simulations in nonzero external field are presented in Sec. IV both for s- and d-wave models. Field-cooled and zero-field-cooled susceptibilities are calculated, together with spatial flux distributions inside the sample. Dynamical properties of the model are studied in Sec. V. In particular, the linear ac susceptibility is calculated both for s- and d-wave models by applying an external ac field. In Sec. VI, possible implications of the obtained simulation results to experiments on high-T_c ceramic superconductors, particularly ac susceptibility and μSR measurements, are discussed in some detail. Section VII is devoted to summary and discussion. Possible consequence of the recent theoretical suggestion of a ''fractional'' or time-reversal-symmetry breaking junction is also discussed.[28,29]

II. MODEL

We are interested in the interloop (intergranular) ordering phenomena of granular superconductors. We suppose that weak links connecting the neighboring grains are distributed sufficiently dense, so that the system can be viewed as an infinite network of Josephson junctions, which are not decomposed into finite clusters. Let us model such ceramic superconductors by a three-dimensional lattice model of a Josephson-junction array with finite self-inductance. When charging effects of the grain can be neglected, the Hamiltonian may be given by[16]

$$\mathscr{H}=-\sum_{\langle ij\rangle} J_{ij}\cos(\theta_i-\theta_j-A_{ij})+\frac{1}{2\mathscr{L}}\sum_p (\Phi_p-\Phi_p^{\rm ext})^2, \tag{2.1}$$

$$\Phi_p=\sum_{\langle ij\rangle}^{p} A_{ij}, \quad A_{ij}=\frac{2\pi}{\phi_0}\int_i^j \mathbf{A}(\mathbf{r})\,d\mathbf{r}, \tag{2.2}$$

where θ_i $(0\leqslant\theta_i<2\pi)$ is the phase of the superconducting order parameter of a grain at the ith site of a simple cubic lattice, $\mathbf{A}$ being the vector potential, ϕ_0 the flux quantum, $\mathscr{L}$ the self-inductance of a loop (an elementary plaquette), and J_{ij} is the Josephson coupling between the ith and jth grains.

Φ_p is the total magnetic flux threading though the pth plaquette, whereas $\Phi_p^{\rm ext}$ is the flux due to a uniform external field applied along the z direction,

$$\Phi_p^{\rm ext}=HS, \quad \text{for } p \text{ on the } \langle xy\rangle \text{ plane,}$$
$$=0, \quad \text{otherwise.} \tag{2.3}$$

The first sum in Eq. (2.1) is taken over all nearest-neighbor bonds on the lattice whereas the second sum is taken over all elementary plaquettes on the lattice. We assume that the quenched randomness occurs only in the distribution of J_{ij}, while the self-inductance of a loop $\mathscr{L}$ and the area of a plaquette S are taken common all over the lattice. Mutual inductance between different loops are neglected. We also assume that the Josephson coupling J_{ij} is independent of temperature and magnetic field. This assumption is more or less justified when the intergranular ordering occurs at a temperature lower than the intragranular superconducting transition.

The first term of Eq. (2.1) represents the standard Josephson-junction energy and the second term represents the spatial energy of current-induced magnetic fields. Dynamical variables of this Hamiltonian are the phase variables at each site, θ_i, and the gauge variables at each bond, A_{ij}. The dynamical nature of the gauge variables A_{ij} leads to the screening effects which were neglected in Ref. 23. Note that the XY-pseudospin Hamiltonian in Ref. 23 is recovered by taking the weak-coupling limit, $\mathscr{L}\rightarrow 0$, since in this limit the induced flux tends to zero due to the second term, and A_{ij}'s are quenched to the external-field values.

In s-wave ceramics, sign of the Josephson coupling is always positive ($J_{ij}>0$), while in d-wave ceramics it could be either positive (0 junction) or negative (π junction) depending on the relative direction of the junction and the crystal grains on both sides. In d-wave ceramics, the sign of J_{ij} is expected to appear randomly since the spatial orientation of each crystal grain would be random.

Recently several theorists suggested that the Josephson junction between d-wave superconductors under certain circumstances might have an energy minimum at some fractional value of the phase difference, neither at 0 or π, as a result of a spontaneous time-reversal-symmetry breaking at the junction.[28,29] Possible consequences of such a ''fractional junction'' will be discussed later in Sec. VII. For the time being, we assume that all junctions consist of either 0 or π junctions in d-wave ceramic superconductors.

In the following, we deal with the following three types of bond distributions. Model I; the spin-glass-type binary ($\pm J$) distribution modeling d-wave ceramics, where J_{ij} takes the values $+J$ (0 junction) and $-J$ (π junction) with equal probability. Model II; the random ''ferromagnetic'' interaction modeling s-wave ceramics, where J_{ij} is always positive but is distributed uniformly between 0 and $2J$. Model II$'$; the pure ''ferromagnetic'' interaction modeling regular s-wave system, where $J_{ij}=J>0$ for all $\langle ij\rangle$.

The model I was first introduced by Domínguez, Jagla, and Balseiro as a model of d-wave ceramic superconductors.[16] These authors simulated the model by the dynamical Langevin method, and found that the linear susceptibility exhibits a paramagnetic behavior in the field-cooling mode, but only a diamagnetic behavior in the zero-field-cooling mode, thus reproducing the PME observed experimentally. In our model I, the numbers of positive and negative couplings are set equal. In this case, half of the total plaquettes are frustrated, and the fraction of the frustrated plaquettes becomes maximal. In real d-wave ceramics, some amount of asymmetry is likely to exist in the distribution of 0 and π junctions. As long as such asymmetry is not so large, however, it would not affect an essential feature of the orbital-glass (chiral-glass) ordering. When there occurs a significant amount of asymmetry, some new features could appear in the ordering process. Such asymmetric case has also been studied by Monte Carlo simulations, and the results will be published elsewhere.[30]

Model II$'$ is a model of conventional s-wave superconductors, and is expected to exhibit a standard normal-super transition. This model was studied by Dusgupta and Halperin by Monte Carlo simulations.[31] Model II is a random version of the model II$'$, modeling s-wave ceramics.

Next, let us examine the global symmetry of the Hamiltonian. In zero external field $\Phi_{\rm ext}=0$, the Hamiltonian (2.1) is invariant under global $U(1)$ gauge transformation, $\theta_i\rightarrow\theta_i+\Delta\theta$, $A_{ij}\rightarrow A_{ij}$, as well as under global Z_2 time-reversal transformation $\theta_i\rightarrow-\theta_i$, $A_{ij}\rightarrow -A_{ij}$. In the pseudospin terminology used in Ref. 23, the $U(1)$ gauge transformation corresponds to global spin rotation, while the Z_2 time-reversal transformation corresponds to global spin reflection. In nonzero external fields $\Phi_{\rm ext}\neq 0$, by contrast, the Hamiltonian is no longer invariant under global Z_2 time-reversal transformation, thought it still remains invariant under global $U(1)$ gauge transformation. In other words, an external magnetic field breaks the time-reversal symmetry only, preserving the gauge symmetry. Due to this symmetry property, a magnetic field is expected to be an excellent probe of chiral order in superconductors or Josephson networks. It is important to realize that a magnetic field in Josephson networks has an entirely different meaning from that in magnets. In magnets, an external magnetic field enters into the Hamiltonian via the Zeeman term and breaks the $SO(2)=U(1)$ spin-rotation symmetry of the Hamiltonian.

In addition to the above global symmetries, the Hamiltonian (2.1) also has a *local* gauge symmetry. In most of our simulations, we adopt the ''temporal gauge,'' following Domínguez, Jagla, and Balseiro.[16] In this gauge, it is convenient to introduce gauge-invariant phase difference on each bond defined by

$$\Psi_{ij}\equiv\theta_i-\theta_j-A_{ij}. \tag{2.4}$$

Then, the dimensionless Hamiltonian may be written in terms of these new variables as

$$\tilde{\mathscr{H}}\equiv\frac{\mathscr{H}}{J}=-\sum_{\langle ij\rangle}\tilde{J}_{ij}\cos\Psi_{ij}+\frac{1}{2\tilde{\mathscr{L}}}\sum_p(\tilde{\Phi}_p-\tilde{\Phi}_p^{\rm ext})^2, \tag{2.5}$$

$$\tilde{\Phi}_p=-\sum_{\langle ij\rangle}^{p}\Psi_{ij}, \tag{2.6}$$

$$\tilde{\Phi}_p^{\rm ext}=h, \quad \text{for } p \text{ on the } \langle xy\rangle \text{ plane,}$$
$$=0, \quad \text{otherwise,} \tag{2.7}$$

where J denotes the typical magnitude of the Josephson coupling and various dimensionless quantities are defined by

$$\widetilde{J}_{ij}=\frac{J_{ij}}{J},\quad h=\frac{2\pi HS}{\phi_0},\quad \widetilde{\mathcal{L}}=\frac{2\pi\mathcal{L}I_c}{c\phi_0}, \tag{2.8}$$

while I_c is the junction maximum critical current defined by

$$I_c=\frac{2\pi cJ}{\phi_0}. \tag{2.9}$$

In the form of Eq. (2.5), it is easy to see that in the strong-coupling limit $\mathcal{L}\to\infty$, our model Hamiltonian reduces to the noninteracting one since the first term becomes the sum of independent bond terms and the second term just vanishes. One may define a local chirality at each plaquette on the lattice by[23–26]

$$\kappa_p=\frac{1}{2\sqrt{2}}\sum_{\langle ij\rangle}^{p}\widetilde{J}_{ij}\sin(\Psi_{ij}), \tag{2.10}$$

where the sum runs over a directed contour along the sides of the plaquette. Note that the chirality is also a gauge-invariant quantity. If the plaquette p is frustrated, the local chirality κ_p tends to take a value around ±1, while if it is unfrustrated, it tends to take a value around zero. Under the global symmetry transformations of the Hamiltonian, chirality behaves as *a pseudoscalar*: Namely, it is invariant under global $U(1)$ gauge transformation, while it changes sign under global Z_2 time-reversal transformation. Due to this symmetry property, *chirality can be regarded as an order parameter of the possible chiral ordering*. Physically, the chirality κ_p is a half (π) vortex, being proportional to the supercurrent circulating around a plaquette p. It takes either positive or negative value depending on whether the supercurrent around a loop circulates either in clockwise or counterclockwise direction.

Local induced flux at a plaquette p is given in the dimensionless form by

$$f_p=\frac{\Phi_p-\Phi_p^{\rm ext}}{\phi_0}. \tag{2.11}$$

It is also a pseudoscalar like chirality, whose sign represents the direction of the current-induced magnetic moment threading the plaquette p. One may also regard the flux as an order parameter of the possible chiral order in view of the fact that the flux has the same symmetry property as the chirality. However, chirality is perhaps more appropriate as an order parameter, since in the weak-coupling limit $\mathcal{L}\to0$ where the chiral-glass transition has been established to take place,[23] the induced flux vanishes identically while the chirality remains nontrivial.

Total magnetization along the z axis normalized per plaquette m, is given by

$$m=\frac{1}{4\pi SN_p}\sum_{p\in\langle xy\rangle}(\Phi_p-\Phi_p^{\rm ext}), \tag{2.12}$$

where the sum is taken over all N_p plaquettes on the $\langle xy\rangle$ plane. One can introduce the corresponding dimensionless quantity by

$$\widetilde{m}\equiv\frac{4\pi S}{\phi_0}m=\frac{1}{N_p}\sum_{p\in\langle xy\rangle}f_p. \tag{2.13}$$

In small fields, the magnetization m may be expanded in powers of the field intensity H as

$$m(H)=m(0)+\chi H+\chi_1H^2+\chi_2H^3+\cdots. \tag{2.14}$$

If there is no symmetry breaking, all terms even in H should vanish in Eq. (2.14). The linear susceptibility χ can also be written as

$$\chi\equiv\frac{dm}{dH}=\frac{d\widetilde{m}}{d(2h)}=\chi_e+\chi_o, \tag{2.15}$$

$$\chi_e=\frac{\pi\widetilde{\beta}N_p}{\widetilde{\mathcal{L}}}[\langle\widetilde{m}^2\rangle]_J-\frac{1}{4\pi}, \tag{2.16}$$

$$\chi_o=-\frac{\pi\widetilde{\beta}N_p}{\widetilde{\mathcal{L}}}[\langle\widetilde{m}\rangle^2]_J, \tag{2.17}$$

where $\langle\cdots\rangle$ represents a thermal average and $[\cdots]_J$ represents a configurational average over the bond distribution, $\widetilde{\beta}$ being defined by

$$\widetilde{\beta}=\widetilde{J}^{-1}=\frac{J}{k_BT}. \tag{2.18}$$

Here, even and odd parts of the susceptibility are denoted by χ_e and χ_o, respectively. The linear susceptibility χ is dimensionless in cgs units. Likewise, the dimensionless nonlinear susceptibility $\widetilde{\chi}_2$ can be written as

$$\widetilde{\chi}_2\equiv\left(\frac{\phi_0}{4\pi S}\right)^2\chi_2=\frac{1}{6}\left(\frac{\phi_0}{4\pi S}\right)^2\frac{d^3m}{dH^3}=\widetilde{\chi}_{2,e}+\widetilde{\chi}_{2,o}, \tag{2.19}$$

$$\widetilde{\chi}_{2,e}=\frac{1}{6}\left(\frac{\pi\widetilde{\beta}N_p}{\widetilde{\mathcal{L}}}\right)^3[\langle\widetilde{m}^4\rangle-3\langle\widetilde{m}^2\rangle^2]_J, \tag{2.20}$$

$$\widetilde{\chi}_{2,o}=-\frac{1}{6}\left(\frac{\pi\widetilde{\beta}N_p}{\widetilde{\mathcal{L}}}\right)^3[4\langle\widetilde{m}^3\rangle\langle\widetilde{m}\rangle-12\langle\widetilde{m}^2\rangle\langle\widetilde{m}\rangle^2+6\langle\widetilde{m}\rangle^4]_J. \tag{2.21}$$

Note that the above χ_2, being proportional to the minus of the third-harmonic component of the ac susceptibility, is sometimes denoted as χ_3 in the literature.

We have performed Monte Carlo simulations based on the standard Metropolis method for the Hamiltonian (2.5) both in zero and nonzero external fields. The lattices studied are simple cubic lattices with $L\times L\times L$ sites with $L=4,8,12$. Free boundary conditions are adopted. For the random models (model I and II), sample average is usually taken over 100–1000 independent bond realizations except for some special cases. In each run, 6×10^4 Monte Carlo steps per spin is generated, with initial 2×10^4 discarded for thermalization. For the regular model (model II′), we have made longer runs, $(102-2)\times10^4$ MCS, which are repeated a few times with different spin initial conditions and different random-number sequences. As mentioned, no particular attention has been paid to the equilibration problem, since the main inter-

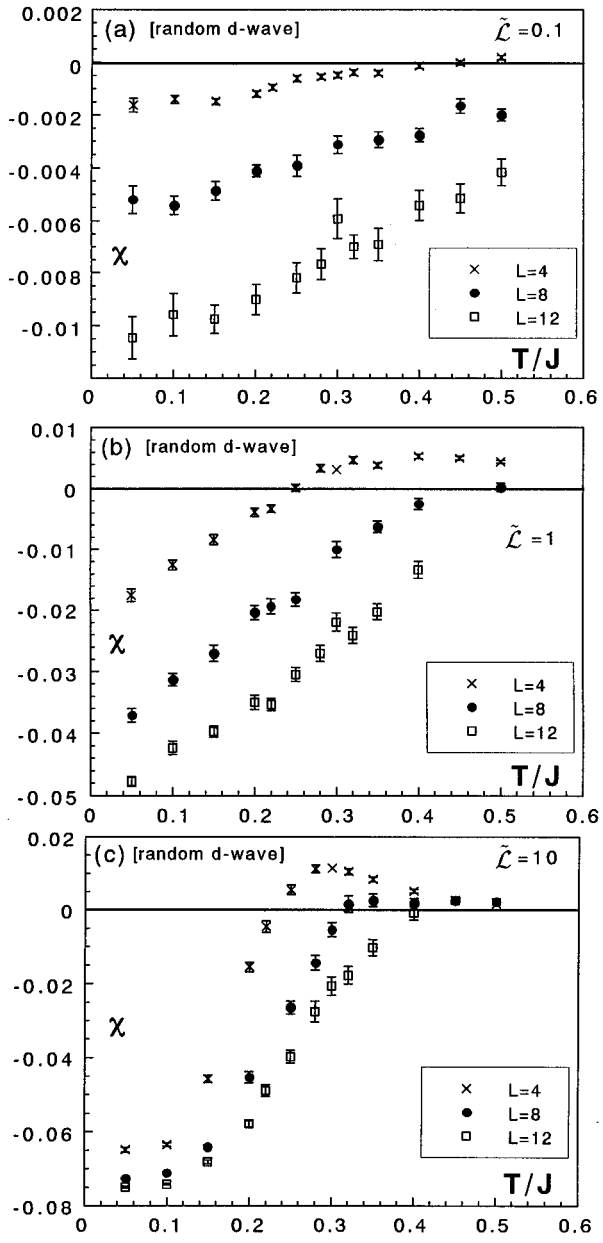

FIG. 1. The temperature and size dependence of the zero-field linear susceptibility χ of model I (d-wave ceramics) for the renormalized inductance $\tilde{\mathcal{L}}$=0.1 (a), 1 (b), and 10 (c). Full Meissner value is equal to $-1/(4\pi)=-0.796...$.

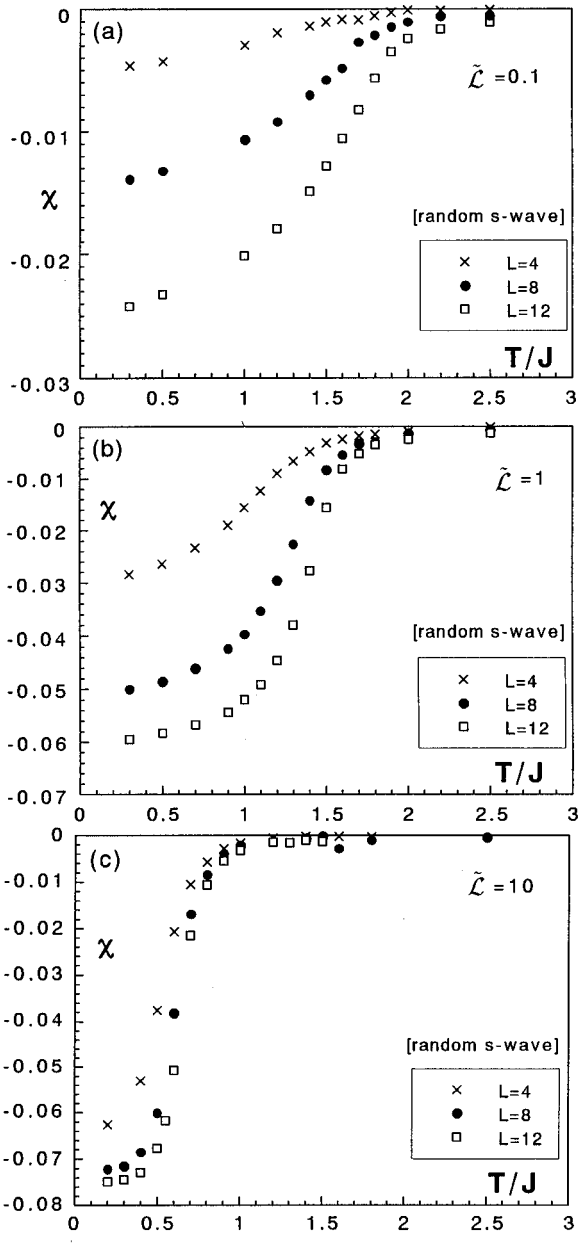

FIG. 2. The temperature and size dependence of the zero-field linear susceptibility χ of model II (s-wave ceramics) for the renormalized inductance $\tilde{\mathcal{L}}$=0.1 (a), 1 (b), and 10 (c). Full Meissner value is equal to $-1/(4\pi)=-0.796...$.

est in the present calculation is not to get full equilibrium properties of the model, but rather to get information connected to the experimental situation.

III. MONTE CARLO SIMULATIONS IN ZERO FIELD

In this section, the results of our Monte Carlo simulations for the three types of bond distributions (I), (II), and (II′) are presented. In Figs. 1(a)–1(c), the temperature and size dependence of the zero-field linear susceptibility χ of model I (d-wave ceramics) is shown for each case of the dimensionless inductance $\tilde{\mathcal{L}}$=0.1, 1, and 10. Here χ is estimated from fluctuations of magnetization in zero external field with use of Eqs. (2.15)–(2.17). The same quantity for model II (s-wave ceramics) is also displayed in Figs. 2(a)–2(c) for each case of $\tilde{\mathcal{L}}$=0.1, 1, and 10. The corresponding χ of the regular s-wave model (model II′) exhibits essentially the same behavior as that of model (II) and is not shown here. From these figures, one sees that both s- and d-wave models exhibit a diamagnetic response ($\chi<0$). This diamagnetic behavior found in d-wave ceramics is in contrast to the paramagnetic behavior observed previously for the XY-pseudospin model of d-wave ceramics where the screening effect was neglected.[23] For both cases of d- and s-wave models, an apparent ordering temperature where χ begins to take a nonzero value decreases with increasing the inductance $\mathcal{L}$. As the system size or the inductance is increased, the value

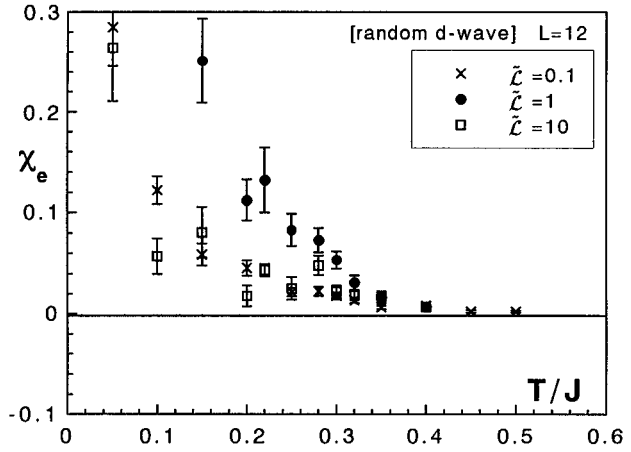

FIG. 3. The temperature and inductance dependence of an even part of the zero-field susceptibility χ_e of model I (d-wave ceramics).

of χ at low temperature tends to the full Meissner value $-1/(4\pi)$.

In fact, there is some subtlety in the sign of χ of the d-wave model. Closer inspection of Fig. 1 shows that χ of the d-wave model takes slightly positive value around the ordering temperature and this behavior is more pronounced for smaller samples. In order to identify the origin of this behavior, an even part of the linear susceptibility χ_e of the model I, defined by Eq. (2.16), is shown in Fig. 3. In contrast to the full susceptibility χ, the even part is found to exhibit a paramagnetic behavior ($\chi_e>0$). For finite systems *in full equilibrium*, any odd quantity should vanish identically, namely, one should have $\chi_o=0$ and $\chi=\chi_e$. Therefore, our observation of the positive χ_e strongly suggests that the observed diamagnetic behavior of χ might in fact be a finite-time effect and that an equilibrium χ of the model I is always positive for finite systems. By contrast, χ_o could take a nonzero value in the thermodynamic limit if some sort of symmetry breaking occurs, and the sign of χ could be negative. Such subtlety found in the sign of χ of the d-wave model may be related to different signs observed experimentally between in the FC and ZFC modes. In sharp contrast to this, no appreciable difference has been observed between χ_e and χ in the case of s-wave models (model II and II′).

The temperature and size dependence of an even part of the zero-field *nonlinear* susceptibility $\chi_{2,e}$ of model I (d-wave ceramics), estimated in zero field with use of Eq. (2.20), is shown in Figs. 4(a)–4(c) for each case of $\tilde{\mathcal{L}}=0.1$, 1 and 10. Due to the numerical difficulty in estimating higher-order quantities, particularly the odd part $\chi_{2,o}$, we could get here only the even part $\chi_{2,e}$ with reasonable accuracy. In any finite system in full equilibrium, one should have $\chi_2=\chi_{2,e}$. As can be seen in Figs. 4(a)–4(c), $\chi_{2,e}$ exhibits a divergent behavior with negative sign. This negative divergence of χ_2 is similar to the one observed in standard spin-glass models,[18] and to the one previously observed for the XY-pseudospin model.[23] As mentioned, to determine whether this divergence is related to a finite-temperature transition in true equilibrium is beyond the scope of the present paper. Note that the specific heat (not shown here) exhibits no appreciable anomaly as in the case of spin glasses.

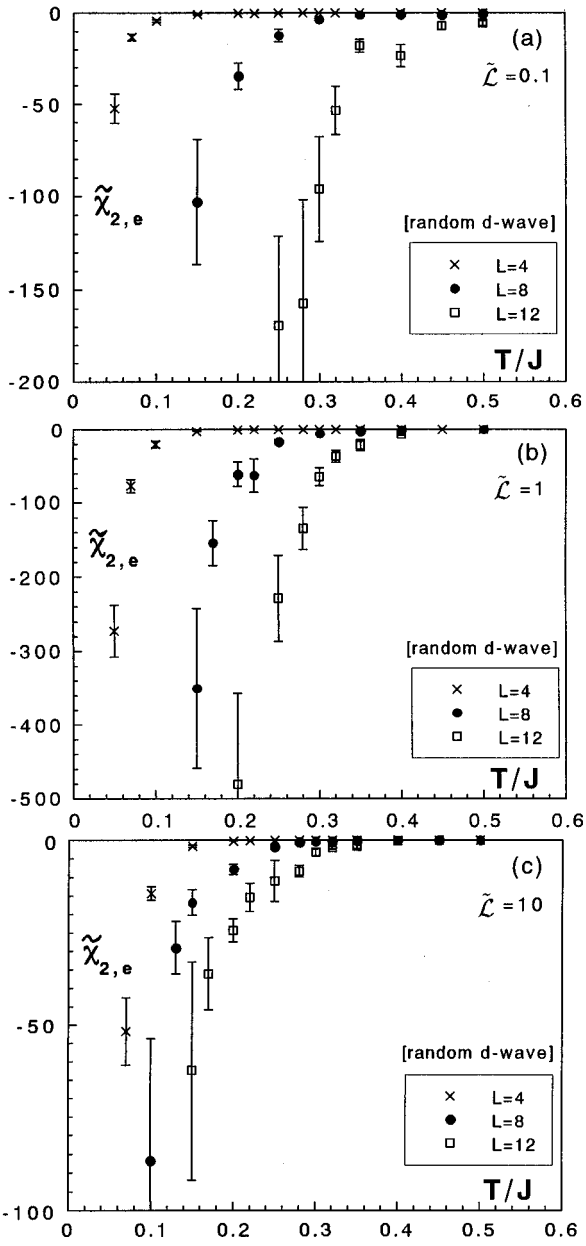

FIG. 4. The temperature and size dependence of an even part of the zero-field nonlinear susceptibility $\tilde{\chi}_{2,e}$ of model I (d-wave ceramics) for the renormalized inductance $\tilde{\mathcal{L}}=0.1$ (a), 1 (b), and 10 (c).

For comparison, we show $\tilde{\chi}_{2,e}$ of the s-wave models (models II′ and II) in Figs. 5 and 6. In these s-wave models, no appreciable difference has been found between $\tilde{\chi}_2$ and $\tilde{\chi}_{2,e}$. The superconducting transition point determined from the specific-heat peak for $L=12$ sample, which is displayed in Fig. 7, is shown by the arrow in these figures. One sees that the nonlinear susceptibilities of these s-wave models exhibit behaviors very different from those of the d-wave model. The value of $\tilde{\chi}_{2,e}$ is orders of magnitude smaller than that of the d-wave model. This is related to the fact that a magnetic field in superconductors is the field conjugate to the chirality, but not conjugate to the phase of the superconducting order parameter itself. The temperature dependence of $\tilde{\chi}_{2,e}$ is also very different from that of the d-wave model:

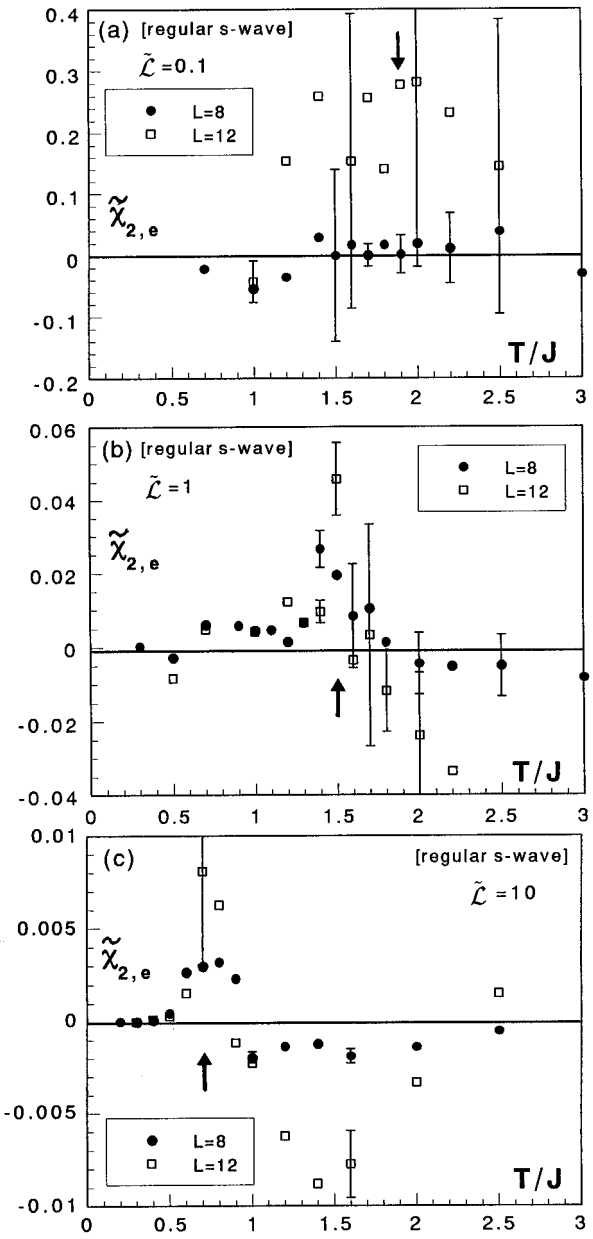

FIG. 5. The temperature and size dependence of an even part of the zero-field nonlinear susceptibility $\tilde{\chi}_{2,e}$ of model II′ (regular s-wave model) for the renormalized inductance $\tilde{\mathcal{L}}=0.1$ (a), 1 (b), and 10 (c). Arrow in the figure indicates the transition point obtained from the specific-heat peak for the $L=12$ lattice.

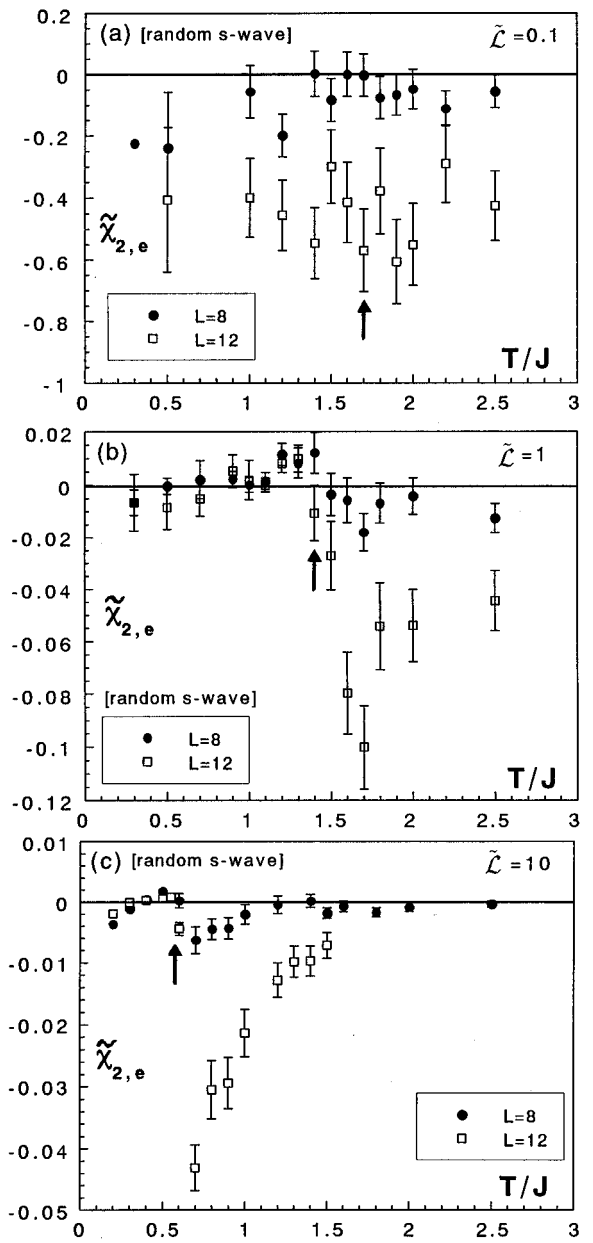

FIG. 6. The temperature and size dependence of an even part of the zero-field nonlinear susceptibility $\tilde{\chi}_{2,e}$ of model II (random s-wave model) for the renormalized inductance $\tilde{\mathcal{L}}=0.1$ (a), 1 (b), and 10 (c). Arrow in the figure indicates the transition point obtained from the specific-heat peak for the $L=12$ lattice.

In the regular s-wave model, $\tilde{\chi}_{2,e}$ has a small positive peak at $T=T_c$, though for larger inductance, a negative dip develops slightly above T_c leading to an asymmetric behavior of $\tilde{\chi}_{2,e}$. As can be seen from Fig. 5, similar asymmetric behaviors of $\tilde{\chi}_{2,e}$ are observed also for the random s-wave model with larger $\mathcal{L}$, while for smaller $\mathcal{L}$ ($\tilde{\mathcal{L}}=0.1$) no appreciable structure can be seen. In any case, the nonlinear susceptibility $\tilde{\chi}_{2,e}$ of the s-wave models exhibits only a very weak anomaly, or no appreciable anomaly, at the superconducting transition point.

A symmetry argument in Sec. I suggests that the divergentlike behavior of χ_2 observed in d-wave ceramics should reflect the random freezing of chirality (circulating supercurrent) or spontaneous flux. In order to see this more directly, we also calculated the Edwards-Anderson-type freezing parameter for chirality defined by

$$q_\kappa=\left(\frac{1}{N_p}\sum_{p\in\langle xy\rangle}[\langle\kappa_p\rangle^2]_J\right)^{1/2}, \tag{3.1}$$

together with a root-mean-square magnitude of the local chirality at each plaquette defined by

$$\overline{\kappa}=\left(\frac{1}{N_p}\sum_{p\in\langle xy\rangle}[\langle\kappa_p^2\rangle]_J\right)^{1/2}, \tag{3.2}$$

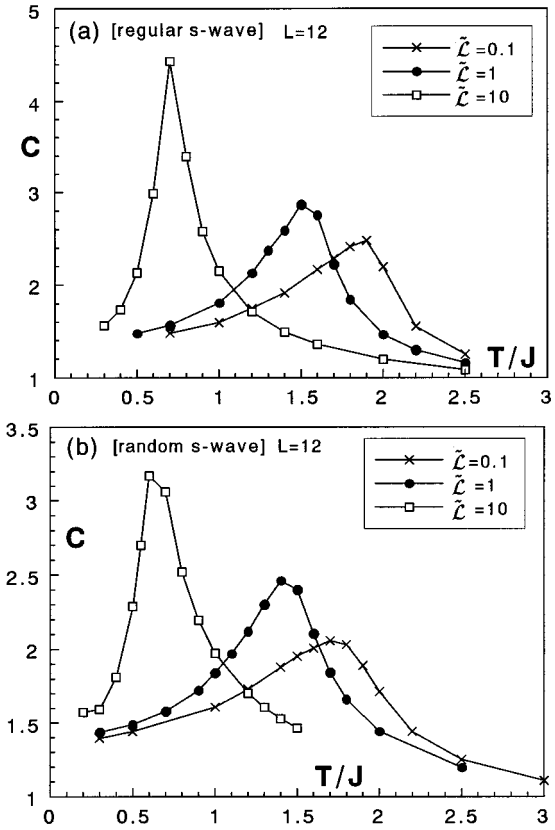

FIG. 7. The temperature and inductance dependence of the specific heat calculated from energy fluctuations of model II′ (regular s-wave model); (a), and of model II (random s-wave model); (b). The lattice size is equal to $L=12$.

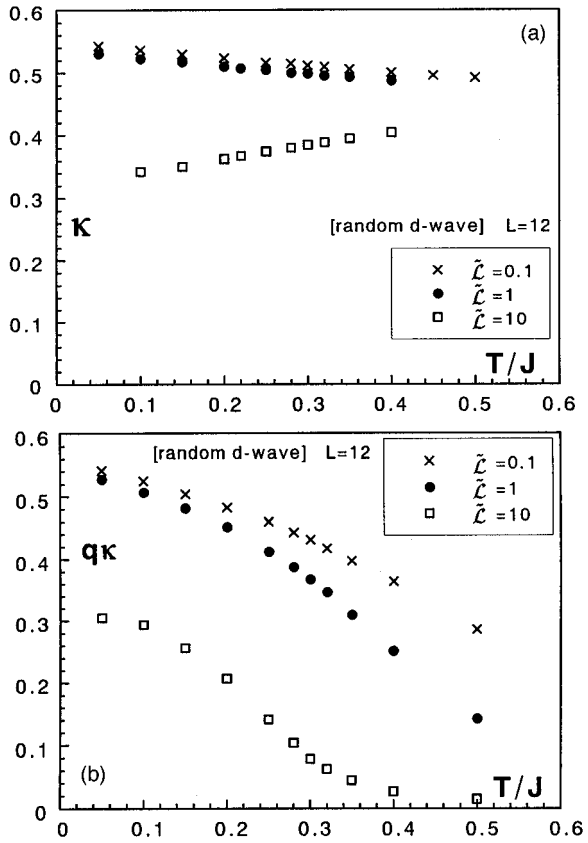

FIG. 8. The temperature and inductance dependence of the root-mean-square magnitude of the local chirality of model I (d-wave ceramics); (a), and of the Edwards-Anderson-type freezing parameter of the chirality of model I; (b).

where $N_p=L(L-1)^2$. The calculated $\overline{\kappa}$ and q_κ are shown in Figs. 8(a) and 8(b), respectively. One sees from Fig. 8(a) that the local chirality takes a finite value even at low temperature, which indicates that the local spontaneous supercurrent indeed exists in the system. (Large values of $\overline{\kappa}$ observed at higher temperatures are due to thermal fluctuations.) At higher temperatures chirality frequently changes its sign leading to small q_κ values, while at lower temperatures it tends to be locked within the observation time leading to an observed growth of q_κ. So, the observed behavior of chirality is consistent with the expectation that the divergent behavior of χ_2 is associated with the random freezing of chirality.

For comparison, we show in Fig. 9 the temperature dependence of $\overline{\kappa}$ and q_κ for model II (s-wave ceramics). In this case, $\overline{\kappa}$ decreases rapidly at lower temperatures indicating that the local supercurrent is largely suppressed, while q_κ remains very small even below T_c indicating that the ordering of the s-wave model is definitely not of chirality origin.

Essentially the same behavior is expected also for spontaneous flux. We also calculated the Edwards-Anderson-type freezing parameter for spontaneous flux, which is defined by

$$q_f=\left(\frac{1}{N_p}\sum_{p\in\langle xy\rangle}[\langle f_p\rangle^2]_J\right)^{1/2}, \tag{3.3}$$

together with a root-mean-square magnitude of the local spontaneous flux at each plaquette.

$$\overline{f}=\left(\frac{1}{N_p}\sum_{p\in\langle xy\rangle}[\langle f_p^2\rangle]_J\right)^{1/2}. \tag{3.4}$$

The calculated $\overline{f}$ and q_f of model I (d-wave ceramics) are shown in Figs. 10(a) and 10(b), respectively. Essentially the same qualitative behavior as that of chirality has been observed.

It should be emphasized here that q_χ and q_f shown above have been estimated only through finite observation time. At the moment, it is not clear whether an apparent ordering temperature observed here for d-wave ceramics corresponds to a true thermodynamic transition. Further careful calculations paying attention to equilibration are required to settle this issue.

IV. MONTE CARLO SIMULATIONS IN NONZERO FIELDS

Although the main interest in the present paper is an intergranular ordering phenomenon *in zero-field limit*, we wish to report in this section some of the results of Monte Carlo simulations performed under finite magnetic fields. The reason of this is that in real experiments one often has to apply a finite magnetic field for detection. We are mainly interested in a weak-field regime where an external flux per loop is smaller than one flux quantum ϕ_0.

One remarkable property of the d-wave model in a weak

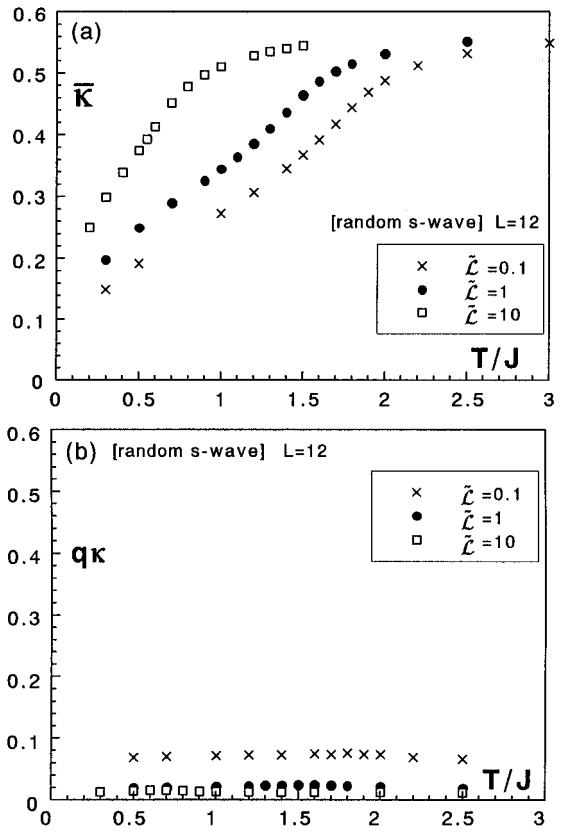

FIG. 9. The temperature and inductance dependence of the root-mean-square magnitude of the local chirality of model II (*s*-wave ceramics); (a), and of the Edwards-Anderson-type freezing parameter of the chirality of model II; (b).

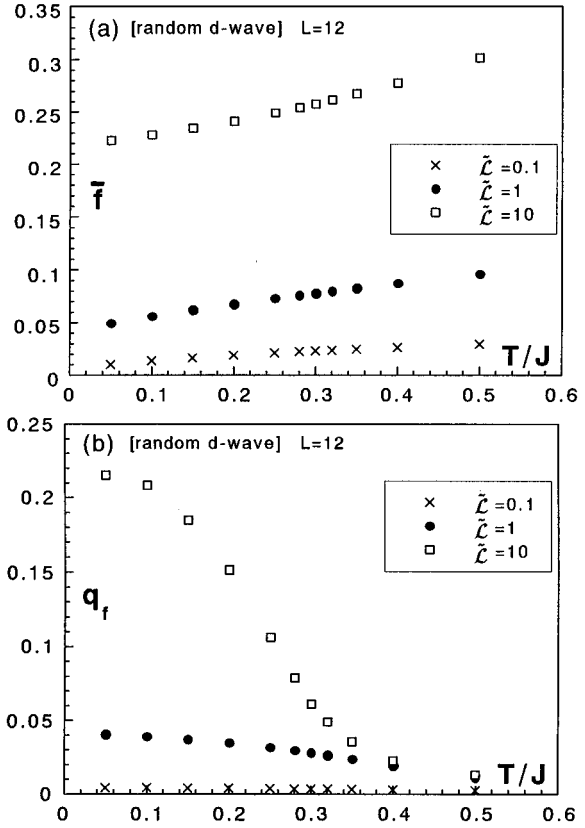

FIG. 10. The temperature and inductance dependence of the root-mean-square magnitude of the local flux of model I (*d*-wave ceramics); (a), and of the Edwards-Anderson-type freezing parameter of the flux of model I; (b).

applied field is the appearance of the PME, as was observed by Domínguez, Jagla, and Balseiro *et al.* We also calculated field-cooled (FC) and zero-field-cooled (ZFC) susceptibilities, $\chi_{\rm FC}$ and $\chi_{\rm ZFC}$, of model I (*d*-wave ceramics) in a weak field, and reproduced this effect. The obtained results are displayed in Fig. 11. The lattice size and the inductance are set to $L=8$ and $\tilde{\mathcal{L}}=1$, while the configurational average have been taken over 50 samples. In the FC runs, the temperature is lowered stepwise under a constant applied field. At each temperature, 6×10^4 MCS runs have been generated, among which initial 2×10^4 MCS are used for thermalization and subsequent 4×10^4 MCS are used for calculating the field-cooled magnetization $m_{\rm FC}$. The field-cooled susceptibility is estimated with use of Eq. (2.15) $\chi_{\rm FC}=\tilde{m}_{\rm FC}/(2h)$. In the ZFC runs, the system is first quenched to a low temperature ($T=0.03J$) in zero field and is thermalized during 6×10^4 MCS. Then, a static dc field is switched on and the temperature is increased stepwise in a constant dc field under the same condition as in the FC runs. The zero-field-cooled susceptibility is estimated from $\chi_{\rm ZFC}=\tilde{m}_{\rm ZFC}/(2h)$.

As can be seen from Fig. 11, a paramagnetic behavior can clearly been seen in the FC runs in the field range $h\lesssim1$, roughly corresponding to $\Phi_{\rm ext}\sim\phi_0/4$. The paramagnetic tendency is more pronounced for smaller fields. By contrast, $\chi_{\rm ZFC}$ remains diamagnetic at low temperatures for any value of the dc fields studied. These observations are essentially the same as the previous observation by Domínguez, Jagla, and Balseiro for different parameter values ($\tilde{\mathcal{L}}=8$ and $c=0.3$, c being the number density of π junctions).[16]

At the end of some of the FC runs ($h=0.1$ and 0.2), we turned off an external field at the lowest temperature reached ($T=0.05J$), and recorded the resulting remanent magnetization $m_{\rm rem}$. A positive value of $m_{\rm rem}$ was obtained, which satisfied the relation $m_{\rm rem}\simeq m_{\rm FC}-m_{\rm ZFC}$, consistent with some experiments on high-T_c ceramics.[32,33] This observation indicates the occurrence of flux trapping in our *d*-wave model.

In earlier simulation, it was suggested that the paramagnetic behavior might occur only for larger inductance $\tilde{\mathcal{L}}\gtrsim1$.[16] In contrast to this suggestion, we observed a clear paramagnetic effect even for smaller inductance. As an example, we show in Fig. 12 the temperature dependence of $\chi_{\rm FC}$ for a very small inductance $\tilde{\mathcal{L}}=0.1$. Still, one has a clear paramagnetic response in the field-cooling mode, although its magnitude is considerably suppressed compared with the $\tilde{\mathcal{L}}=1$ case. It is likely that the PME persists even for infinitesimal inductance at least in the present model.[34]

In this connection, it should be noted that, by analyzing the properties of a frustrated π loop consisting of only single π junction, Sigrist and Rice found that there exists a critical value of the inductance, $\tilde{\mathcal{L}}_c=1$, above which spontaneous supercurrent arises but below which there is no spontaneous supercurrent.[8] In Appendix A, we made a similar analysis for a frustrated π loop consisting of *four* junctions, nothing but

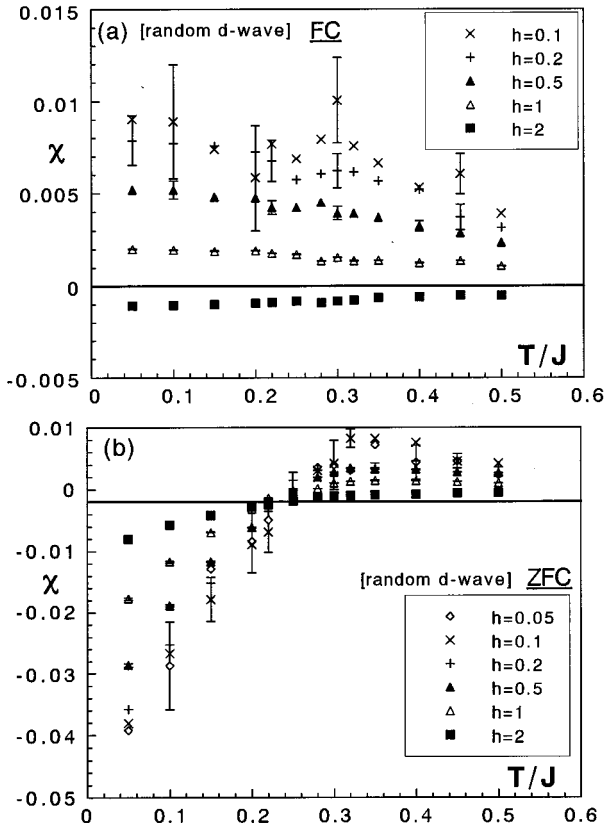

FIG. 11. The temperature dependence of the field-cooled susceptibility (a) and of the zero-field-cooled susceptibility (b) of model I (d-wave ceramics) for several values of external dc fields. The lattice size is equal to $L=8$ and the renormalized inductance is equal to $\widetilde{\mathcal{L}}=1$.

an elementary frustrated plaquette of our present lattice model. It is found that there is no critical value of $\mathcal{L}$ in this case ($\mathcal{L}_c=0$) and spontaneous supercurrent arises even for infinitesimal inductance in contrast to the case analyzed by Sigrist and Rice. This observation naturally explains why the PME has been observed even for very small inductance in our present simulation.

In Fig. 13, the temperature and field dependence of $\chi_{\rm FC}$ and $\chi_{\rm ZFC}$ of the model II (s-wave ceramics) is shown. Again, we set $\widetilde{\mathcal{L}}=1$ and $L=8$. The procedure of the calculation is the same as in the case of model I. The lowest temperature in the ZFC runs has been chosen to be $T=0.3J$. As expected, the response here is always diamagnetic. Furthermore, there is no appreciable difference between $\chi_{\rm FC}$ and $\chi_{\rm ZFC}$ for smaller dc fields ($h\lesssim 0.2$): These χ values also agree with χ calculated from magnetization fluctuations in zero field in Sec. III (see Fig. 2). Remanent magnetization $m_{\rm rem}$ were also calculated at the end of some of the FC runs ($h=0.1$ and 0.2) as in the case of model I. Within statistical errors $m_{\rm rem}$ turned out to be zero, which is consistent with the relation $m_{\rm rem}=m_{\rm FC}-m_{\rm ZFC}$.

For completeness, we also simulated the case of rather strong external field $h=10$ for model II (s-wave ceramics), corresponding to the case of more than one flux quantum per plaquette ($h=2\pi$). With this amount of external field, nature of the ordering appears to be considerably changed from the

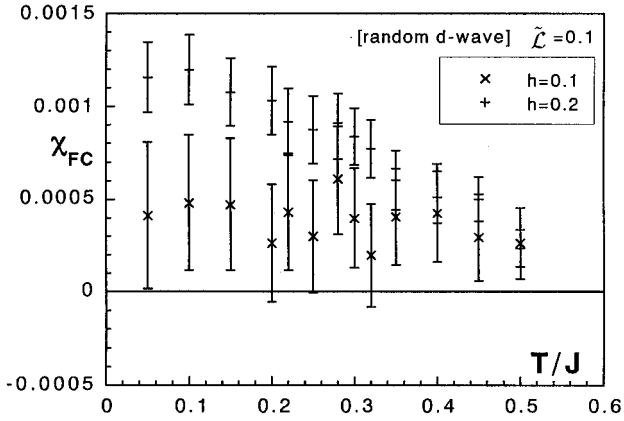

FIG. 12. The temperature dependence of the field-cooled susceptibility of model I (d-wave ceramics) with a smaller inductance $\widetilde{\mathcal{L}}=0.1$ for several values of external dc fields. The lattice size is equal to $L=8$.

zero-field case: The calculated magnetization becomes slightly positive at low temperatures without any appreciable anomaly in the specific heat. Chirality takes fairly large values at low temperatures even for the s-wave model, reflecting the existence of frustration due to magnetic fields.

Note that the nature of ordering under magnetic fields is

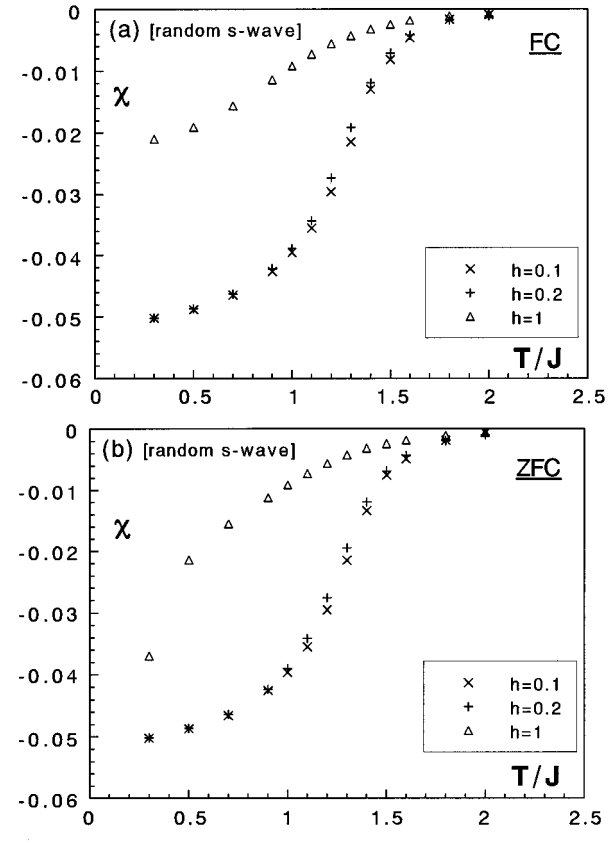

FIG. 13. The temperature dependence of the field-cooled susceptibility (a) and of the zero-field-cooled susceptibility (b) of model II (s-wave ceramics) for several values of external dc fields. The lattice size is equal to $L=8$ and the renormalized inductance is equal to $\widetilde{\mathcal{L}}=1$.

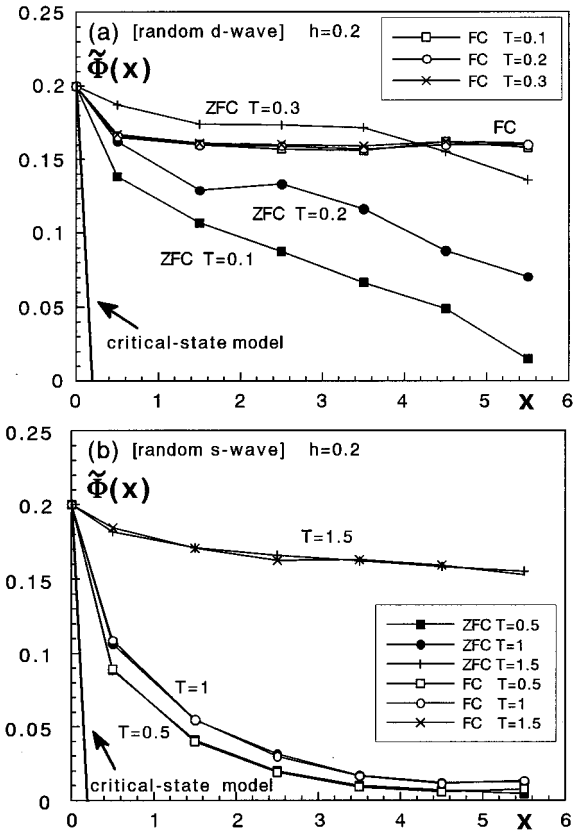

FIG. 14. Spatial flux distributions at several temperatures inside the sample of model I (d-wave ceramics); (a), and of model II (s-wave ceramics); (b), for both cases of the field-cooling (FC) and zero-field-cooling (ZFC) runs. Applied dc field is equal to $h=0.2$. Distance from the surface of the sample, x, is measured in units of lattice spacing. The data are averaged over 40 independent bond realizations and over four equivalent directions ($\pm x$ and $\pm y$ axes). The flux distribution calculated by applying the phenomenological critical-state model to the ZFC runs is also shown (see text and Appendix B).

very different from that in zero field. In particular, in the case of d-wave model, there cannot be a chiral-glass transition under magnetic fields. This is simply due to the fact that the Hamiltonian under nonzero magnetic fields (gauge-glass Hamiltonian) does *not* possess a discrete Z_2 time-reversal symmetry any longer, only a continuous $U(1)$ gauge symmetry being left. A possible ordered state under magnetic fields, a vortex-glass state,[35] is characterized by the spontaneous breaking of this $U(1)$ gauge symmetry under fields. Although a stable vortex-glass phase has been expected in the absence of screening,[36] a recent calculation suggests that in the presence of screening there might not exist a stable vortex-glass phase in external fields.[22] Anyway, the application of an external field of order $\phi_0/4$ per loop completely changes the nature of zero-field intergranular orderings (chiral-glass ordering in d-wave ceramics or standard superconducting transition in s-wave ceramics).

We also studied the spatial distribution of flux inside the sample. In Figs. 14(a) and 14(b), such spatial flux distributions obtained in the FC and ZFC runs are displayed for each case of d- and s-wave ceramics (models I and II) as a function of x, a distance from the surface in units of lattice spacing. For both cases of d- and s-wave models, we set $L=12$, $\tilde{\mathcal{L}}=1$ and $h=0.2$, the configuration average being taken over 40 samples and four equivalent directions along the $\pm x$ and $\pm y$ axes. In the ZFC runs, on switching on an external field, flux gradually enters into the sample from the surface, while in the FC runs flux is gradually squeezed out of the sample from the surface. One sees from Fig. 14 that the flux distribution of the s-wave model does not depend on FC/ZFC modes, and thus, is expected to be fairly close to the equilibrium distribution. By contrast, in the case of the d-wave model, some difference is observed between the FC and ZFC runs: In the FC runs, flux is distributed rather uniformly fully penetrating into the sample, while in the ZFC runs, flux penetration remains incomplete at low temperatures due to the flux pinning. [Here note that the spatial flux distribution of each individual sample of the d-wave model is much more erratic reflecting the particular distribution of frustrated plaquettes inside the sample. Rather smooth distribution displayed in Fig. 14(a) has been obtained only after the sample average.]

One phenomenological model often used in giving spatial flux distributions inside the sample is the so-called critical-state model:[37–42] It is a strongly nonequilibrium model in which the induced supercurrent inside the sample is assumed to be either $\pm I_c$ or 0 depending on its history. A large supercurrent inside the sample is supposed to be maintained by the strong pinning effect. Spatial flux distribution calculated by applying such a critical-state model to the ZFC runs of the present lattice model is also displayed in the figure. (Some of the derivation is given in Appendix B.) Note that the critical-state model is a macroscopic model making no distinction between s-wave and d-wave pairing symmetries, and gives the same flux distribution for both cases. From the figure, one sees that the flux distribution observed in our present simulation is much more gradual than the one expected from the critical-state model: Namely, net supercurrents circulating inside the sample are much smaller than those expected in the critical-state model. It means that flux pinning is certainly happening in our d-wave model, but its magnitude is much weaker than the type of strong pinning assumed in the critical-state model.

V. SIMULATIONS OF AC SUSCEPTIBILITIES

So far, we have concentrated our attention on the static properties of the model. In the present section, we study the dynamic properties of the model, particularly the linear ac susceptibility, by Monte Carlo technique. While Monte Carlo simulations involve no real dynamics, one can still expect that they give useful information about the long-time behavior of the system.

From the experimental side, measurements of ac susceptibilities have been one of the useful tools to study conventional as well as high-T_c superconductors.[2,3,41,43–49] It has been known that in these superconducting materials the real part of the linear ac susceptibility χ' shows a diamagnetic behavior, whereas the imaginary part χ'' shows a maximum below a critical temperature. On increasing the ac-field intensity, or on decreasing the ac-field frequency, the maxima of χ'' tend to shift toward lower temperature. Several models, including the critical-state model,[37–42] superconducting-loop

model,[43,48,50–52] and superconducting-glass model,[1–3,47] have been proposed to account for those and other properties of superconducting materials.

In this section, we simulate model I (random d-wave model) and II$'$ (regular s-wave model) under oscillating ac fields of magnitude $H_{\rm ac}$ and of frequency ω,

$$H = H_{\rm ac}\cos(\omega t), \tag{5.1}$$

in order to obtain the dynamical properties of the model, particularly the linear ac susceptibility $\chi = \chi' + i\chi''$. It should be noted that the ac susceptibilities of a similar Josephson-network model with finite self-inductance were numerically investigated by Wolf and Majhofer.[53] However, these authors dealt with the s-wave system in two dimensions, and also applied very strong ac fields corresponding to $H_{\rm ac}S \simeq 100\phi_0$. In the present paper, we simulate both the s-wave and d-wave systems in three dimensions, and apply much weaker ac fields corresponding to $H_{\rm ac}S < \phi_0$.

Via the dimensionless magnetization defined by Eq. (2.13), $\tilde{m}$, the real and imaginary parts of the ac susceptibility $\chi'(\omega)$ and $\chi''(\omega)$ are calculated as

$$\chi'(\omega) = \frac{1}{\pi h_{\rm ac}} \int_0^{2\pi} \tilde{m}(t)\cos(\omega t)\, d(\omega t),$$
$$\chi''(\omega) = \frac{1}{\pi h_{\rm ac}} \int_0^{2\pi} \tilde{m}(t)\sin(\omega t)\, d(\omega t), \tag{5.2}$$

where t denotes the Monte Carlo time and the dimensionless ac-field intensity $h_{\rm ac}$ is normalized as in Eq. (2.8). In this section, we have chosen the gauge where all the bond variables A_{ij} along the z direction are fixed to be zero, and have set the dimensionless inductance to be $\tilde{\mathcal{L}} = 1$. The sample average is taken over 10–20 independent bond realizations. Other conditions are the same as in the previous sections.

$\chi(\omega)$ has been estimated following the procedure in Refs. 54 and 55: Namely, at the beginning of a given Monte Carlo run at each temperature, we first switch on the ac field (5.1). Then, after waiting for initial t_0 Monte Carlo steps per spin (MCS), we start to monitor the time variation of the magnetization, t_0 being chosen so that all transient phenomena can be considered extinct. We set t_0 to be 2×10^4 MCS in our following simulations. After passing the point $t = t_0$, $\tilde{m}(t)$ is averaged over typically 200–1500 periods, each period containing t_T MCS ($t_T = 2\pi/\omega$). The real and imaginary parts of the susceptibility are then extracted via Eq. (5.2).

The results of our calculations on model I (random d-wave model) with $L = 8$ are presented in Fig. 15. We set $h_{\rm ac} = 0.1$, corresponding to $\simeq 0.016$ flux quantum per plaquette. Smaller values of $h_{\rm ac}$ have turned out to leave the results almost unchanged. As can be seen from Fig. 15, the real part $\chi'(\omega)$ shows a diamagnetic behavior. Since the ac susceptibilities for small ω would be closer to the zero-field-cooled susceptibilities rather than the field-cooled susceptibilities, the diamagnetic behavior observed here seems consistent with our dc results in Sec. IV. As expected, on decreasing ω, $\chi'(\omega)$ approaches the static susceptibility $\chi(\omega = 0)$.

One sees from the figure that both the real part χ' and the imaginary part χ'' show a significant ω dependence. In particular, the location of the peak of χ'' shifts toward lower

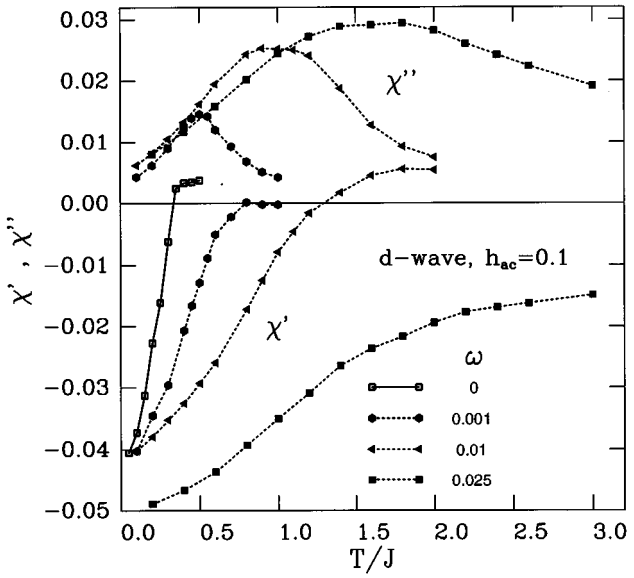

FIG. 15. The temperature dependence of the real and imaginary parts of the linear ac susceptibility, $\chi'(\omega)$ and $\chi''(\omega)$, of model I (d-wave ceramics). The dimensionless parameters are $h_{\rm ac} = 0.1$ and $\tilde{\mathcal{L}} = 1$, and the system size is $L = 8$. Open squares, black hexagons, triangles, and squares represent $\omega = 0$ (static case), 0.001, 0.01, and 0.025, respectively. The error bars are smaller than the symbols.

temperature very quickly, and the shape of the peak sharpens up. In fact, the observed behavior of χ'' is reminiscent of the χ'' recently observed in the spin-glass model (three-dimensional $\pm J$ Ising model),[55] and suggests the existence of a slow dynamics in these systems. Qualitatively similar ω dependence has also been observed in experiments, but to much less extent.[2,46,47] Presumably, the observed quantitative

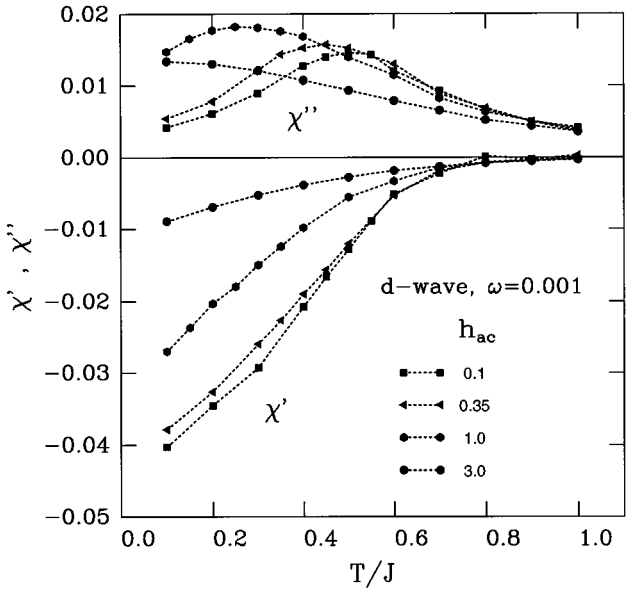

FIG. 16. The temperature and ac-field intensity dependence of the real and imaginary parts of the linear ac susceptibility, $\chi'(\omega)$ and $\chi''(\omega)$, of model I (d-wave ceramics) with $L = 8$, $\tilde{\mathcal{L}} = 1$, and $\omega = 0.001$. The squares, triangles, hexagons, and circles represent $h_{\rm ac} = 0.1$, 0.35, 1.0, and 3.0, respectively.

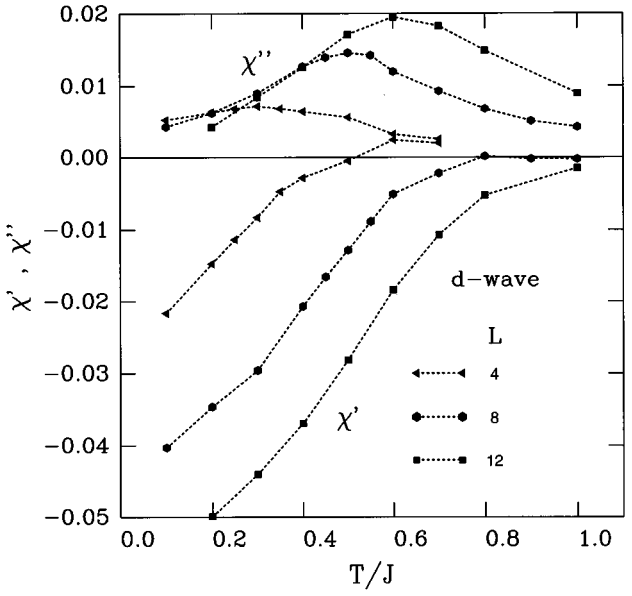

FIG. 17. The temperature and size dependence of the real and imaginary parts of the linear ac susceptibility, $\chi'(\omega)$ and $\chi''(\omega)$, of model I (d-wave ceramics) with $h_{ac}=0.1$, $\tilde{\mathcal{L}}=1$, and $\omega=0.001$. The triangles, hexagons, and squares represent $L=4$, 8, and 12, respectively.

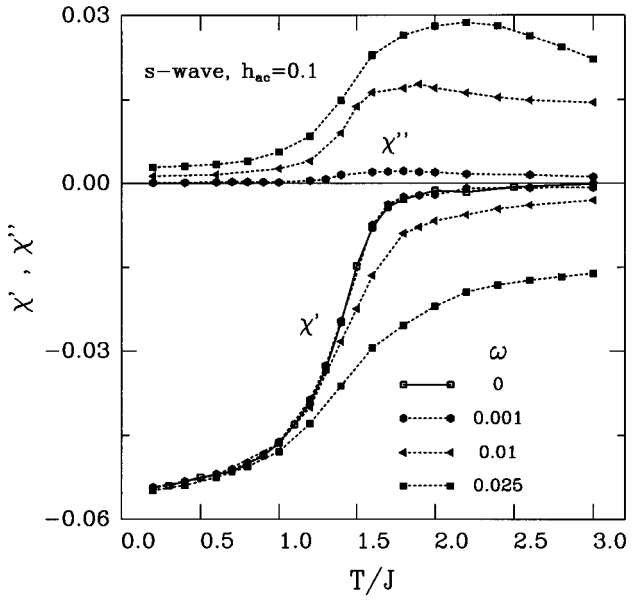

FIG. 18. The temperature dependence of the real and imaginary parts of the linear ac susceptibility, $\chi'(\omega)$ and $\chi''(\omega)$, of model II′ (regular s-wave model). The dimensionless parameters are $h_{ac}=0.1$ and $\tilde{\mathcal{L}}=1$, and the system size is $L=8$. Open squares, black hexagons, triangles, and squares represent $\omega=0$ (static case), 0.001, 0.01, and 0.025, respectively.

difference simply reflects the fact that our ac fields correspond to extremely rapid oscillations in real time.

The h_{ac} dependence of χ of model I is shown in Fig. 16. Here we set $L=8$ and $\omega=0.001$. On decreasing h_{ac}, the peak of χ'' moves toward higher temperature. This tendency is consistent with experimental results[3,39,41,43,44,47,48] and also with a few phenomenological models, e.g., critical-state model[39,40] and superconducting-loop model.[52] Thus, a simple lattice model of a Josephson-junction array with self-inductance is found to reproduce qualitative features of ac susceptibility experiments. The size dependence of χ of model I has also been studied for $h_{ac}=0.1$ and $\omega=0.001$, and the results are presented in Fig. 17. The peak of χ'' moves toward higher temperature as the system size is increased.

Our results for model II′ (regular s-wave model) with $L=8$ and $h_{ac}=0.1$ are shown in Fig. 18. As expected, the real part shows a diamagnetic behavior while the imaginary part exhibits a broad maximum. If one compares the results with the corresponding results of model I in Fig. 15, several points are noticed. At higher frequencies, there is very little difference between the χ of the d- and s-wave models. In fact, at the highest frequency studied $\omega=0.025$, χ of the two models are similar even quantitatively. On the other hand, at lower frequencies, clear differences shows up: First, the magnitude of χ'' of the s-wave model becomes an order of magnitude smaller than that of the d-wave model, indicating that the d-wave model exhibits much stronger dissipation in the low-frequency regime. This tendency is expected to be more enhanced if one goes further to lower frequencies. Second, the ω dependence observed in the peak position of χ'' as well as in the onset temperature of diamagnetism in χ' is much less in the s-wave case than in the d-wave case. Slow dynamics which give rise to the significant ω dependence in the d-wave model seem to be absent in the s-wave model.

Unfortunately, in the present dynamical simulation we could not calculate with reasonable accuracy the *nonlinear* ac susceptibility, and thus, could not directly probe the possible chiral-glass ordering in d-wave ceramics. Nevertheless, a close similarity observed between the χ'' of d-wave ceramics and that of the spin glass as well as strong dissipation observed in the low-frequency regime of d-wave ceramics are consistent with the chiral-glass picture discussed in the previous sections based on the static results.

VI. IMPLICATIONS TO EXPERIMENTS ON HIGH-T_c CERAMICS

In this section, on the basis of the results obtained in the previous sections, we wish to discuss several possible implications to experiments on high-T_c ceramic superconductors. One of the most prominent characteristics of the chiral-glass ordering is a negative divergence of the zero-field nonlinear susceptibility. Experimentally, χ_2 is often measured by the ac technique, in which one applies an oscillating ac field, $h(t)=h_{ac}\cos(\omega t)$, and measures the coefficient of the third-harmonic component of the response, $\chi(3\omega)h_{ac}\cos(3\omega t)$. Then the nonlinear susceptibility χ_2 is related to $\chi(3\omega)$ via $\chi_2 \approx -\chi(3\omega)$. Although the predicted divergence of χ_2 is *a static property in zero field*, $\omega \to 0$ and $h_{ac} \to 0$, one needs to apply a detection field of finite amplitude h_{ac} and finite frequency ω in real ac measurements. Here it is important to make sure that h_{ac} and ω are kept sufficiently small: For example, in order to probe intrinsic zero-field critical properties, the value of h_{ac} should certainly be much smaller than $\phi_0/4$ per loop. Under certain circumstances, this requirement could be rather severe. If the mean diameter of a loop (comparable to grain size) is of order 10 μm, then the value of h_{ac} should be much smaller than 50 mG. If the mean diameter of

a loop is of order 1 μm, this condition is somewhat loosened to $h_{ac} \ll 5$ G. Perhaps, in the larger h_{ac} or ω regime, the difference between the d- and s-wave models would be washed out as seen in Sec. V, and the resulting nonequilibrium state may well be described by the macroscopic critical-state model. The negative divergence of χ_2 could only be seen in equilibrium, or at least near equilibrium condition in zero-field limit.

It should be mentioned here that the critical-state model also gives rise to a peak in χ_2 *if one further assumes the temperature dependence of the Josephson coupling* J_{ij}.[37–42] However, such a peak expected in the critical-state model with temperature dependent J_{ij} is a rounded one not related to any singularity, unlike the divergent behavior observed in our model I. (Note that, since we did not consider any temperature dependence of J_{ij} in our present model, the negative divergence of χ_2 observed in the present simulation is not explicable by the critical-state model anyway.)

At the moment, there is at least one experimental result which appears to support the chiral-glass picture. Thus, Matsuura *et al.* recently measured the nonlinear susceptibility of ceramic samples of $YBa_2Cu_4O_8$ consisting of single-crystal grains of diameter less than 1 μm.[49] Two well separate transitions were observed: The one at a higher temperature associated with the intragranular ordering and the other at a lower temperature with the intergranular ordering.[33] While both χ_{FC} and χ_{ZFC} were diamagnetic without any paramagnetic behavior, Matsuura *et al.* observed a negatively divergent anomaly of χ_2 at the intergranular transition point with using the ac field of $h_{ac}=10$ mG and $f=\omega/(2\pi)=0.1$ Hz. This rather sharp anomaly was interpreted by these authors as arising from an intrinsic intergranular critical phenomenon, possibly associated with the chiral-glass transition. Further detailed experimental studies, including static and dynamic scaling analyses,[56] are highly desirable. It is also worthwhile to try systematic experimental surveys for other types of high-T_c ceramics including Bi-Sr-Ca-Cu-O and Y-Ba-Cu-O 1-2-3 compounds.

The PME may also be regarded as an attribute of d-wave ceramic superconductors. While observation of the PME may be regarded as a hint of the nontrivial pairing symmetry,[8] the converse is not true: Namely, as discussed below, anisotropic (d wave) ceramic superconductors may well exhibit diamagnetic behavior only as many experiments on high-T_c ceramics have shown. It should also be noted that Thompson *et al.* recently reported the observation of the PME in conventional superconductors, niobium, and ascribed it to the strong flux pinning at the surface as well as to the geometric shape of the sample.[57]

Since the PME has clearly been observed in the present model, the reason why the PME is observed so rarely in real experiments should be attributed to the effects not taken into account in our model. One possible cause might be a diamagnetic contribution coming from *intragranular* supercurrents which have totally been neglected in our model. Another source may be the possible field and temperature dependence of the Josephson coupling J_{ij} which have also been neglected in the present model.

In any case, it should be emphasized that the mere sign of χ depends on many nonuniversal details of the system. Thus, the mere sign of χ is also not an indicator of the chiral-glass state: In the chiral-glass state in real ceramics, χ_{FC} could be either positive or negative. It is also completely possible that the state showing a positive χ_{FC}, which one may regard as being in the orbital-glass state, does *not* exhibit a negative divergence of χ_2 and is *not* in the chiral-glass state. In fact, as can been seen from Fig. 11(a), a positive χ_{FC} is realized well above the intergranular ordering temperature, which indicates that the intragranular superconductivity alone is enough to cause the positive χ_{FC}.[8,17]

In sharp contrast to the sign of χ, the negative divergence of χ_2 is expected to be a *universal property* which should be robust to most of the details of the system as long as there occurs an intergranular chiral-glass ordering. Since the behavior of χ_2 of the s-wave system has turned out to be very different from that of the d-wave system, one may use the behavior of χ_2 at the intergranular transition point as an indicator of the pairing symmetry as proposed in Ref. 23.[58]

One other experimental method which might give useful information on the possible chiral-glass ordering is muon spin relaxation (μSR). The chiral-glass state is characterized by frozen-in circulating supercurrents and orbital moments *in zero external field*. Such moments are distributed spatially random, but remain stable over a long period of time. Since the origin of possible time-reversal-symmetry breaking comes from weak links, not from the bulk superconducting order parameter, it is essential to perform measurements on ceramic samples containing sufficiently many weak links, rather than on high-quality single crystals.

VII. SUMMARY AND DISCUSSION

Intergranular ordering phenomena of ceramic superconductors are studied by Monte Carlo simulations on a three-dimensional lattice model of a Josephson-junction array with finite self-inductance. Both cases of d-wave and s-wave systems are studied. In the case of d-wave ceramics, intrinsic frustration effects combined with quenched randomness lead to the glassy behavior reminiscent of the spin glass even in zero field.

The main finding of the present simulation is that the nonlinear susceptibility of d-wave ceramics exhibits a negative divergence indicative of the occurrence of a cooperative phase transition. The calculated Edwards-Anderson-type freezing parameter of chirality and of flux has shown that this cooperative phenomenon is associated with the random freezing of chirality or of spontaneous flux (chiral-glass transition proposed in Ref. 23). Thus, a global Z_2 time-reversal symmetry appears to be broken at least within a finite observation time of simulations. It remains to be seen whether the observed cooperative phenomenon is a true thermodynamic phase transition at a finite temperature or a dynamical freezing phenomenon reflecting slow dynamics associated with a zero-temperature transition.

Dynamical simulations on the linear ac susceptibility have revealed a close similarity between the ordering of d-wave ceramics and that of the spin glass, particularly in the behavior of the imaginary part of the ac susceptibility. It is also found that the d-wave model exhibits much stronger dissipation than the s-wave model in the low-frequency regime.

Although our present simulation of d-wave ceramics has been made for a lattice model with some specific bond dis-

tribution ($\pm J$ distribution), the above physical conclusion would not depend on the details of the bond distribution. Essential ingredients are (i) three-dimensional connectivity of weak links, (ii) frustration, (iii) randomness, and (iv) time-reversal symmetry in the Hamiltonian (chiral degeneracy).

In sharp contrast to such glassy behavior found in d-wave ceramics, s-wave models (both random and regular) exhibit a conventional normal-super phase transition accompanied with a sharp anomaly in the specific heat. This transition is associated with a spontaneous breaking of global $U(1)$ gauge symmetry which has nothing to do with the chirality. The zero-field nonlinear susceptibility shows a behavior very different from that of d-wave ceramics: It exhibits only a very weak anomaly (positive peak, asymmetric behavior, etc.) or no appreciable anomaly at all at the superconducting transition point.

Recent experiments strongly suggest that cuprate high-T_c superconductors are anisotropic or unconventional superconductors characterized by the non-s-wave pairing symmetry.[5–7] At present the most promising symmetry appears to be $d_{x^2-y^2}$. There also exists a strong experimental evidence that heavy fermion superconductors are also anisotropic superconductors.[59] Although we have described our model I as d-wave ceramics in the present paper, essentially the same physical results are expected for other types of non-s-wave symmetries such as p wave.[60] The essential ingredient is that the superconducting order parameter has nodes on the Fermi surface where it changes sign. In that sense, even an extended-s-wave state could exhibit the same behavior as long as nodes appear on the Fermi surface (there are eight such nodes in contrast to four in the case of d wave). For all these anisotropic superconductors, the nature of the chiral-glass ordering would be rather insensitive to the details of the order parameter: For example, ceramics with $d_{x^2-y^2}$ and d_{xy} pairing symmetries would exhibit essentially the same ordering behavior.

Recently, Sigrist and co-workers and Tanaka and Kashiwaya argued that although the bulk order parameter of high-T_c superconductors does not break the time-reversal symmetry ($d_{x^2-y^2}$ waves), the one at the Josephson junction or at the interface might break the time-reversal symmetry *spontaneously*.[28,29] It should be emphasized that in these scenarios the time-reversal symmetry of the junction Hamiltonian itself is preserved, i.e., $E(\Psi)=E(-\Psi)$ or $I(\Psi)=-I(-\Psi)$, and only the ''state'' spontaneously breaks the time-reversal symmetry. In such a case, although the resulting junction-Hamiltonian no longer has a local energy minimum at 0 or π, symmetry properties of the Hamiltonian remain the same as the model studied here, both $U(1)$ and Z_2 symmetries being kept intact. Thus, one expects essentially the same type of chiral-glass transition characterized by the spontaneous breaking of global Z_2 time-reversal symmetry even for such fractional-junction array.

Recent finding of anisotropic superconductivity in high-T_c cuprates and heavy fermions opens up a valuable opportunity to study thermodynamic properties of a new state of matter. Clearly, further experimental as well as theoretical studies are required to fully explore this interesting possibility.

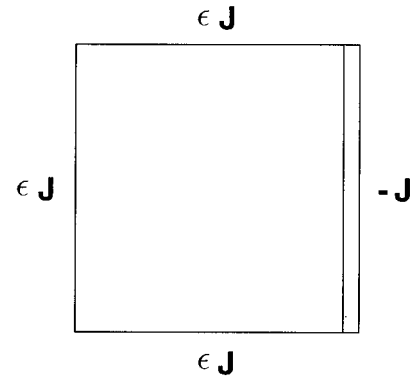

FIG. 19. An isolated frustrated loop consisting of four junctions, one of which is a π junction of magnitude $-J$ and the other three are 0 junctions of magnitude ϵJ with $0<\epsilon<\infty$. The case $\epsilon=1$ corresponds to an elementary frustrated plaquette of our model I, while the case $\epsilon=\infty$ corresponds to the frustrated loop with single π junction analyzed by Sigrist and Rice (Ref. 8).

ACKNOWLEDGMENTS

The author is grateful to Professor M. Matsuura, Professor T. Ishida, Dr. M. Sigrist, Dr. T. Onogi, Dr. K. Kuboki, Dr. Y. Tanaka, and Dr. D. Domínguez for discussions and correspondence. M. S. Li thanks the Japan Society for Promotion of Science for the financial support. The numerical calculation has been performed on the FACOM VPP500 at the supercomputer center, Institute of Solid State Physics, University of Tokyo.

APPENDIX A: GROUND-STATE PROPERTIES OF AN ISOLATED FRUSTRATED PLAQUETTE

In this appendix, we analyze the ground-state properties of an isolated frustrated plaquette, an elementary unit of our lattice model. The plaquette consists of four bonds (junctions) among which one is a π junction with negative coupling constant $-J<0$, and other three are 0 junctions with positive coupling constant $\epsilon J>0$: See Fig. 19. Here, an arbitrary positive number $0<\epsilon<\infty$ has been introduced, while our original model corresponds to $\epsilon=1$. By this extension, a frustrated loop with a single π junction previously analyzed by Sigrist and Rice[8] can be incorporated into the model simply by taking the limit $\epsilon\rightarrow\infty$. For simplicity an external magnetic field is assumed to be zero, though an extension to finite fields is straightforward.

In the temporal gauge, the dimensionless Hamiltonian (energy) of a plaquette is given

$$\tilde{\mathcal{H}}=\cos\Psi_1-\cos\Psi_2-\cos\Psi_3-\cos\Psi_4 + \frac{1}{2\tilde{\mathcal{L}}}(\Psi_1+\Psi_2+\Psi_3+\Psi_4)^2, \tag{A1}$$

where we denote the gauge-invariant phases as Ψ_1 at π junction, and as $\Psi_2\sim\Psi_4$ at 0 junctions. Other notations are the same as in Sec. II. Minimizing $\tilde{\mathcal{H}}$ with respect to $\Psi_1\sim\Psi_4$, we get four coupled equations. After a little algebra, one sees that the ground-state configuration should satisfy the relations

$$\Psi_2=\Psi_3=\Psi_4=\Psi, \quad \Psi_1=\sin^{-1}(-\epsilon\,\sin\Psi), \tag{A2}$$

with Ψ being determined by solving the equation

$$-\epsilon\,\sin\Psi=y(\Psi)\equiv 3\Psi+\sin^{-1}(\epsilon\,\sin\Psi)-\pi. \tag{A3}$$

By analyzing the functional form of $y(\Psi)$, one sees that if ϵ is smaller than three, this equation always has doubly degenerate solutions $\Psi=\pm\Psi^*$ which correspond to the chiral states with mutually opposite chiralities or fluxes. A spontaneous moment (either + or −) arises for an arbitrary value of the inductance. If ϵ is larger than three, on the other hand, there appears a finite critical value of the inductance $\tilde{\mathcal{L}}_c(\epsilon)=1-(3/\epsilon)$: For a larger inductance $\tilde{\mathcal{L}}>\tilde{\mathcal{L}}_c(\epsilon)$, there again exist doubly degenerate solutions $\Psi=\pm\Psi^*$, while for smaller inductance $\tilde{\mathcal{L}}<\tilde{\mathcal{L}}_c(\epsilon)$, only one trivial solution exists at $\Psi=0$ corresponding to the achiral state without spontaneous supercurrent or flux. An elementary frustrated plaquette of our original lattice model ($\epsilon=1$) corresponds to the case where spontaneous moment arises for an arbitrary value of inductance, while a single-junction loop analyzed by Sigrist and Rice ($\epsilon=\infty$) corresponds to the case where spontaneous moment does not occur for smaller inductance $\tilde{\mathcal{L}}<\tilde{\mathcal{L}}_c(\epsilon)$. Indeed, if one sets $\epsilon=\infty$ in the expression of $\tilde{\mathcal{L}}_c$, one recovers the critical value obtained by Sigrist and Rice,[8] $\tilde{\mathcal{L}}_c=1$.

Physically, the above result suggests that spontaneous orbital moments could arise, in principle, even for smaller inductance, particularly in the type of ceramic samples where weak links of nearly the same magnitude are distributed densely.

In the case $\epsilon=1$, chirality and spontaneous flux are calculated in the limits of small and large inductances as

$$\kappa\approx\pm 1, \quad f\approx\pm\frac{\tilde{\mathcal{L}}}{2\sqrt{2}\pi}, \quad \text{for } \tilde{\mathcal{L}}\ll 1, \tag{A4}$$

$$\kappa\approx\pm\frac{\sqrt{2}\pi}{\tilde{\mathcal{L}}}, \quad f\approx\pm\frac{1}{2}, \quad \text{for } \tilde{\mathcal{L}}\gg 1. \tag{A5}$$

Note that, for smaller inductance, spontaneous flux remains nonzero but becomes small as can be seen from Eq. (A4). Therefore, in real ceramic samples where one has an additional diamagnetic contribution from intragranular supercurrents, which has been neglected in the present model, a small paramagnetic contribution arising from the intergranular supercurrents might easily be masked. Therefore, in practice, moderately large inductance would be necessary to observe the paramagnetic behavior.

APPENDIX B: CRITICAL-STATE MODEL

In this appendix, the phenomenological critical-state model[37–42] is applied to our lattice-model Hamiltonian, to calculate the spatial flux distribution inside the sample. Assuming that the local physical quantities depend only on the distance from the surface of the sample x, which is measured in units of lattice spacing d, the Maxwell equation can be written as

$$\frac{dB_z(x)}{d(xd)}=-\frac{4\pi}{c}\,j_y(x), \tag{B1}$$

where $B_z(x)$ is a magnetic flux density and $j(x)$ is a local current density. Here a magnetic field is applied along the z direction and the current flows along the y direction. With setting $I(x)=d^2j(x)$ and $\mathcal{L}=4\pi S/d$, Eq. (B1) can be rewritten in the dimensionless form as

$$\frac{d\tilde{\Phi}(x)}{dx}=-\tilde{\mathcal{L}}\,\frac{I(x)}{I_c}. \tag{B2}$$

In the critical-state model, one simply assumes that the current inside the sample is equal to either $\pm I_c$ or 0 depending on the history. In the case where a static external field is switched on as in the case of ZFC runs, $I(x)$ should be equal to I_c or 0. Remember that in our lattice model I_c has been chosen constant independent of magnetic field (and of temperature), which corresponds to the simplest version of the critical-state model (Bean's model[37]). Thus, setting $I(x)=I_c$ or 0, one has

$$\frac{d\tilde{\Phi}(x)}{dx}=-\tilde{\mathcal{L}} \quad \text{or} \quad 0, \tag{B3}$$

which gives the flux distribution *independent of temperature*,

$$\tilde{\Phi}(x)=h-\tilde{\mathcal{L}}x, \quad \text{for } 0<x<h/\tilde{\mathcal{L}},$$
$$=0, \quad \text{for } x>h/\tilde{\mathcal{L}}. \tag{B4}$$

---

*On leave from Warsaw Institute of Physics, Poland.

[1] K. A. Müller, M. Takashige, and J. G. Bednorz, Phys. Rev. Lett. **58**, 1143 (1987).

[2] Z. Koziol, Physica C **159**, 281 (1989).

[3] K. Park, J. J. Kim, and J. C. Park, Solid State Commun. **71**, 743 (1989).

[4] C. Rossel, Y. Maeno, and I. Morgenstern, Phys. Rev. Lett. **62**, 681 (1989).

[5] D. A. Wollman, D. J. van Harlingen, W. C. Lee, D. M. Ginsberg, and A. J. Leggett, Phys. Rev. Lett. **71**, 2134 (1993); D. J. van Harlingen, Rev. Mod. Phys. **67**, 515 (1995).

[6] C. C. Tsuei, J. R. Kirtley, C. C. Chi, L. S. Yu-Jahnes, A. Gupta, T. Shaw, J. Z. Sun, and M. B. Ketchen, Phys. Rev. Lett. **73**, 593 (1994).

[7] A. Mathai, Y. Gim, R. C. Black, A. Amar, and F. C. Wellstood, Phys. Rev. Lett. **74**, 4523 (1995).

[8] M. Sigrist and T. M. Rice, J. Phys. Soc. Jpn. **61**, 4283 (1992); J. Low Temp. Phys. **95**, 389 (1994); Rev. Mod. Phys. **67**, 503 (1995).

[9] P. Svedlindh, K. Niskanen, P. Nordblad, L. Lundgren, B. Lönnberg, and T. Lundström, Physica C **162–164**, 1365 (1989).

[10] W. Braunisch, N. Knauf, G. Bauer, A. Kock, A. Becker, B. Freitag, A. Grütz, V. Kataev, S. Neuhausen, B. Roden, D. Khomskii, D. Wohlleben, J. Bock, and E. Preisler, Phys. Rev. B **48**, 4030 (1993); W. Braunisch *et al.*, Phys. Rev. Lett. **68**, 1908 (1992); D. Khomskii, J. Low Temp. Phys. **95**, 205 (1994).

[11] S. Riedling, G. Bräuchle, R. Lucht, K. Röhberg, H. v. Löhneysen, H. Claus, A. Erb, and G. Müller-Vogt, Phys. Rev. B **49**, 13 283

(1994); R. Lucht, H. v. Löhneysen, H. Claus, M. Kläser, and G. Müller-Vogt, Phys. Rev. B **52**, 9724 (1995).

[12] L. N. Bulaevskii, V. V. Kuzii, and A. A. Sobyanin, JETP Lett. **25**, 290 (1977).

[13] V. B. Geshkenbein, A. I. Larkin, and A. Barone, Phys. Rev. B **36**, 235 (1987).

[14] B. I. Spivak and S. A. Kivelson, Phys. Rev. B **43**, 3740 (1991).

[15] F. V. Kusmartsev, Phys. Rev. Lett. **69**, 2268 (1992); J. Supercond. **5**, 463 (1992).

[16] D. Domínguez, E. A. Jagla, and C. A. Balseiro, Phys. Rev. Lett. **72**, 2773 (1994).

[17] J. Magnusson, J.-O. Andersson, M. Björnander, P. Nordblad, and P. Svedlindh, Phys. Rev. B **51**, 12 776 (1995); J. Magnusson, M. Björnander, L. Pust, P. Svedlindh, P. Nordblad, and T. Lundström, *ibid*. **52**, 7675 (1995).

[18] Among researchers of spin glasses, there now seems to be a consensus that a three-dimensional XY spin glass does *not* exhibit an equilibrium spin-glass transition of the conventional type at any finite temperature (Refs. 19–21). Then, a true thermodynamic intergranular phase transition with broken $U(1)$ gauge symmetry seems rather unlikely in d-wave ceramic superconductors. One may suspect that the coupling between the XY-spin-like phase variables and the electromagnetic fields (gauge fields), which is absent in XY spin glasses but present in superconductors, might stabilize an ordering. In fact, however, such coupling to the gauge fields make the otherwise long-ranged interaction between vortices short ranged (Ref. 22), and makes the $U(1)$ gauge-symmetry-breaking phase transition even more unlikely. Nevertheless, spin-glass-type random ordering of the phase of the superconducting order parameter has occasionally been discussed: See, for example, S. V. Panyukov and A. D. Zaikin, Physica B **203**, 527 (1994). In this paper, the authors claimed on the basis of an XY spin-glass Hamiltonian and replica trick the existence of a stable spin-glass-like state characterized by a nonzero Edwards-Anderson order parameter associated with the phase degree of freedom of the Cooper-pair wave function, $Q_{\alpha\beta}=\langle\exp[i(\theta_\alpha-\theta_\beta)]\rangle$ (θ denotes the phase, α and β are replica indices). Although such a state characterized by nonzero $Q_{\alpha\beta}$ is certainly possible in the mean-field limit, numerical simulations on an XY spin glass have revealed that this does not occur *in three dimensions* at least for the symmetric distributions of nearest-neighbor bonds (Refs. 19–21).

[19] For a review on spin glasses, see, e.g., K. Binder and A. P. Young, Rev. Mod. Phys. **58**, 801 (1986); K. H. Fischer and J. D. Hertz, *Spin Glasses* (Cambridge University Press, Cambridge, 1991).

[20] S. Jain and A. P. Young, J. Phys. C **19**, 3913 (1986).

[21] B. W. Morris, S. G. Colborne, M. A. Moore, A. J. Bray, and C. Canisius, J. Phys. C **19**, 1157 (1986).

[22] H. S. Bokil and A. P. Young, Phys. Rev. Lett. **74**, 3021 (1995).

[23] H. Kawamura, J. Phys. Soc. Jpn. **64**, 711 (1995).

[24] H. Kawamura, in *Computational Physics as a New Frontier in Condensed Matter Research*, edited by H. Takayama, M. Tsukada, H. Shiba, F. Yonezawa, M. Imada, and Y. Okabe (The Physical Society of Japan, Tokyo, 1995), p. 209.

[25] H. Kawamura, Phys. Rev. B **51**, 12 398 (1995); J. Phys. Soc. Jpn. **61**, 3062 (1992); H. Kawamura and M. Tanemura, *ibid*. **60**, 608 (1991).

[26] H. Kawamura and M. Tanemura, J. Phys. Soc. Jpn. **54**, 4479 (1985); Phys. Rev. B **36**, 7177 (1987).

[27] J. Villain, J. Phys. C **10**, 4793 (1977).

[28] M. Sigrist, D. B. Bailey, and R. B. Laughlin, Phys. Rev. Lett. **74**, 3249 (1995); K. Kuboki and M. Sigrist (unpublished).

[29] Y. Tanaka and S. Kashiwaya (unpublished).

[30] H. Kawamura (unpublished).

[31] C. Dusgupta and B. I. Halperin, Phys. Rev. Lett. **47**, 1556 (1981).

[32] A. P. Malozemoff, L. Krusin-Elbaum, D. C. Cronemeyer, Y. Yeshrun, and F. Holtzberg, Phys. Rev. B **38**, 6490 (1988).

[33] M. Kawachi, M. Hagiwara, K. Koyama, and M. Matuura, J. Phys. Soc. Jpn. **63**, 3405 (1994).

[34] Recently, paramagnetic $\chi_{\rm FC}$ was observed for even smaller inductance value $\tilde{\mathcal{L}}=0.01$ [D. Domínguez (private communication)].

[35] M. P. A. Fisher, Phys. Rev. Lett. **62**, 1415 (1989); D. S. Fisher, M. P. A. Fisher, and D. A. Huse, Phys. Rev. B **43**, 130 (1991).

[36] D. A. Huse and H. S. Seung, Phys. Rev. B **42**, 1059 (1990); J. D. Reger, T. A. Tokuyasu, A. P. Young, and M. P. A. Fisher, *ibid*. **44**, 7147 (1991); M. Cieplak, J. R. Banavar, M. S. Li, and A. Khurana, *ibid*. **45**, 786 (1992); M. J. P. Gingras, *ibid*. **45**, 7547 (1992).

[37] C. P. Bean, Rev. Mod. Phys. **36**, 31 (1964).

[38] Y. B. Kim, C. F. Hempstead, and A. R. Strnad, Phys. Rev. Lett. **9**, 306 (1962); Phys. Rev. **129**, 528 (1963).

[39] T. Ishida and R. B. Goldfarb, Phys. Rev. B **41**, 8937 (1990).

[40] K.-H. Müller, Physica C **159**, 717 (1989); K.-H. Müller, J. C. MacFarlane, and R. Driver, Physica C **158**, 69 (1989); **158**, 366 (1989).

[41] T. Ishida, T. Mikayama, K. Okuda, M. Azuma, Z. Hiroi, and M. Takano, in *Advances in Superconductivity VII* (Springer-Verlag, Berlin, 1995).

[42] L. Ji, R. H. Sohn, G. C. Spalding, C. J. Lobb, and M. Tinkham, Phys. Rev. B **40**, 10 936 (1989).

[43] T. Ishida and M. Mazaki, J. Appl. Phys. **52**, 6798 (1981).

[44] T. Ishida and M. Mazaki, Jpn. J. Appl. Phys. **26**, L1296 (1987).

[45] A. Saulov and D. Dorman, Appl. Phys. Lett. **53**, 2680 (1988).

[46] A. P. Malozemoff, T. K. Worthington, Y. Yeshrun, and F. Holtzberg, Phys. Rev. B **38**, 7203 (1988).

[47] C. Giovannella, C. Lucchini, B. Lecuyer, and L. Fruchter, IEEE Trans. Magn. **25**, 3521 (1989).

[48] W. Win, L. E. Wenger, J. T. Chen, E. M. Logothetis, and R. E. Soltis, Physica C **172**, 233 (1990).

[49] M. Matsuura, M. Kawachi, K. Miyoshi, M. Hagiwara, and K. Koyama, J. Phys. Soc. Jpn. **64**, 4540 (1995).

[50] C. D. Jeffries, Q. H. Lam, Y. Kim, L. C. Bourne, and A. Zettl, Phys. Rev. B **37**, 9840 (1989); Q. H. Lam and C. D. Jeffries, *ibid*. **39**, 4772 (1989); C. D. Jeffries, Q. H. Lam, Y. Kim, C. M. Kim, A. Zettl, and P. M. Klein, *ibid*. **39**, 11 526 (1989).

[51] T. Xia and D. Stroud, Phys. Rev. B **39**, 4792 (1989).

[52] Th. M. Nieuwenhuizen and J. Pankert, Europhys. Lett. **11**, 457 (1990).

[53] T. Wolf and A. Majhofer, Phys. Rev. B **47**, 5383 (1993).

[54] M. Z. Cieplak, T. R. Gawron, and M. Cieplak, Phys. Rev. B **39**, 6757 (1989).

[55] M. S. Li, T. Q. Hung, and M. Cieplak, J. Phys. (France) I **6**, 1 (1996).

[56] When one is allowed to neglect the screening effects, the critical exponents at such an intergranular chiral-glass transition have been estimated as $\gamma\simeq 3-3.6$, $\nu\simeq 1.5$, $\eta\simeq -0.4-$, $z\nu\simeq 7.9$ (Ref. 23). It may well occur that the screening effects modify these exponent values.

[57] D. J. Thompson, M. S. M. Minhaj, L. E. Wenger, and J. T. Chen, Phys. Rev. Lett. **75**, 529 (1995).

[58] Strictly speaking, the sign of χ_2 is an indicator of the existence of

π junctions. Possible occurrence of π junctions in standard s-wave superconductors due to magnetic impurities have been discussed theoretically in Refs. 12, 14, and 15, while its reality was questioned in Ref. 8.

[59] R. A. Fisher, S. Kim, B. F. Woodfield, N. E. Phillips, L. Taillefer, D. G. Hinks, M. Levy, and B. K. Sarma, Phys. Rev. Lett. **62**, 1411 (1989); K. Hasselbach, L. Taillefer, and J. Flouquet, *ibid*. **63**, 93 (1989); G. M. Luke, A. Keren, L. P. Le, W. D. Wu, Y. J. Uemura, D. A. Bonn, L. Taillefer, J. D. Garrett, *ibid*. **71**, 1466 (1993).

[60] If, on the other hand, the bulk superconducting order parameter breaks the time-reversal symmetry as in the case of the so-called B phase of UPt_3 (Ref. 59), a chiral-glass transition is not expected in the granular sample, since the junction Hamiltonian already breaks the time-reversal symmetry *energetically*.